Journal of Materials Chemistry C

ROYAL SOCIETY OF CHEMISTRY

PAPER

View Article Online
View Journal | View Issue

Cite this: J. Mater. Chem. C, 2025, 13, 10413

Imidazo[1,5-*a*]pyridine–benzilimidazole conjugated (donor–π–acceptor) greenish-yellow fluorophores and their applications in white light-emitting diodes, acidochromism and anticounterfeiting†

Bhabana Priyadarshini Debata,[a] Sabita Patel *[a] and Sivakumar Vaidyanathan *[b]

This work reports the design and synthesis of three D–π–A push–pull fluorophores (**BPy-1**, **BPy-2**, and **BPy-FL**) featuring flexible phenyl or rigid and sterically hindered diethylfluorene moieties. The role of spacer units in modulating their photophysical properties has been analyzed through DFT analysis and experimental findings. All the fluorophores are characterized by excellent intramolecular charge transfer (ICT) and positive solvatochromism with a large Stokes shift (~7000 cm^{-1}) due to the presence of the N1 functionalized benzilimidazole acceptor and the 1,3-diphenylimidazo[1,5-*a*]pyridine donor attached through a phenyl spacer in the case of **BPy-1** and **BPy-2** and a diethyl fluorene spacer in **BPy-FL**. **BPy-1** and **BPy-2** show strong greenish-yellow emission at around 520 nm in solution, solid, and thin-film matrices with a good quantum yield (~70%). **BPy-FL** exhibits blue emission (λ_{max} = 458 nm) in THF solution and intense greenish-yellow emission (λ_{max} = 510 nm) in the solid state with an absolute quantum yield of 93%. The fluorophore **BPy-FL** shows aggregation-induced emission (AIE) and hybridized local charge transfer (HLCT) characteristics. The DFT analysis depicts the energy matching of high-lying triplet states (T_4–T_5) with the first excited singlet state, which is beneficial for hot exciton harvesting. Due to their strong greenish-yellow emissions in the solid state, these fluorophores are employed as organic downconverter materials in hybrid white light-emitting diodes (LEDs). Among the fabricated white LEDs, the LED consisting of **BPy-FL** demonstrated excellent luminous efficiency with a high color rendering index (CRI) of ~90% and CIE coordinates (0.37,0.32) almost identical to the NTSC standard. Due to the bipolar nature of the imidazole ring, all these fluorophores display remarkable on–off–on fluorescence behavior in response to alternate addition of acid and base in solution as well as in a thin film state. These fluorophores are, therefore, successfully utilized as fluorescent pH sensors to detect volatile organic compounds with high acidity (an orange emissive state at pH < 4 and a greenish-yellow emissive state at pH > 4). The sensing mechanism has been studied through ^{1}H-NMR and DFT analyses. The potential of these fluorophores in anticounterfeiting applications has been studied, and due to intense emission in the solid state of **BPy-FL**, its application in latent fingerprint (LFP) detection has also been explored.

Received 17th March 2025,
Accepted 8th April 2025

DOI: 10.1039/d5tc01152c

rsc.li/materials-c

Introduction

Organic fluorophores with donor–π–acceptor (D–π–A) push–pull systems have drawn much interest because of their potential uses in sensors, fluorescence imaging, nonlinear optical materials, solid-state lasers, and light-emitting diodes (LEDs).[1–4] Benzilimidazole (BI) has retained its appeal over the last 20 years, especially for lighting and sensing applications.[5–7] BI is an essential building block for the D–π–A design strategies for various sensing and optoelectronic applications. Its imidazole ring has two electrically distinct N atoms (N1 and N3): one electron rich and another electron deficient on opposite sides of the C2 atom. This bipolar nature makes it possible to create luminophores with moderate intramolecular charge transfer (ICT), non-linear optical luminescence, phosphorescence, and fluorescence. Because of their vast

[a] Department of Chemistry, National Institute of Technology Rourkela, Rourkela-769008, Odisha, India. E-mail: sabitap@nitrkl.ac.in
[b] Department of Chemistry, Indian Institute of Technology, Kandi, Sangareddy, 502285, Hyderabad, Telangana, India. E-mail: vsiva@chy.iith.ac.in

† Electronic supplementary information (ESI) available. See DOI: https://doi.org/10.1039/d5tc01152c

potential in a variety of domains, including fluorescent sensors and optoelectronic applications, bipolar imidazole derivatives have attracted a lot of attention from both academia and industry as stable and effective luminous materials.[8–12] They have remarkable charge-transport characteristics and an excellent photoluminescence quantum yield. Substituted BI can act as either a soft electron-withdrawing or a soft electron-donating partner when attached to form a D–π–A framework, depending upon the connectivity at the C2 position.[8,11] Due to their ease of synthesis, rigid structure, thermal stability, bipolar nature, excellent emission behavior, aggregation-induced emission (AIE) feature, and possibility for different structural changes at the N1 and C2 locations of the benzilimidazole ring, these materials are increasingly used as organic emissive materials in a variety of optical, analytical and optoelectronic applications.

Solid-state lighting (SSL) technologies, which include LEDs, have the potential to replace traditional lighting sources like incandescent and fluorescent lights due to their environmental and financial benefits.[13–16] SSL technologies are increasingly replacing conventional light sources due to their advantages of low power consumption, longevity, directionality, resilience, and compact size. SSL aims to produce white light with consistent illumination and suitable color coordinates for general lighting and display purposes.[17,18] By substituting organic materials for conventional phosphors in hybrid LEDs, the solid-state lighting sector could avoid becoming overly reliant on costly rare-earth-containing compounds.[14,19,20] The quicker reaction time of the organic materials compared to the traditional phosphors is another advantage for applications such as visible light communications.[21–23] White light may be produced in inorganic and organic LEDs using various techniques. Three techniques are mainly used for producing white light in inorganic LEDs: (a) combining red, green, and blue monochromatic photons; (b) utilizing ultraviolet (UV) LEDs as excitation sources for blue, green, and red phosphors; and (c) using blue LEDs to excite green, red, or yellow phosphors.[13,22,24,25] The first technique (a) is the least successful because of the cost-effectiveness, challenges with consistent color mixing, and unsuitability for large-scale production. Down-conversion phosphors have been employed as the luminous materials in techniques (b) and (c), where the luminescence conversion results from the Stokes shift between the light absorbed and re-emitted by an organic material or an inorganic phosphor.[26–28] Researchers have utilized phosphors based on silicon-based oxynitride and nitride compounds, aluminates, sulfides, and orthosilicates. However, most oxide-based phosphors have minimal visible spectrum absorption, making it difficult to couple them with blue LEDs. Organic phosphors may be readily spin-cast and dip-coated across vast substrates, offering a wide range of color tunability.[29–31] A hybrid inorganic/organic LED design is an intriguing way to address this problem. This approach applies an organic material with an absorbance band that matches the emission wavelength of the inorganic structure of a blue-emissive inorganic UV LED.[32,33] The organic material converts the lower-energy yellow-red light and high-energy blue luminescence that the inorganic LED emits into an energy-down-converter that produces high-quality white output.[13,34] The III-nitride alloy system, which can produce light from the ultraviolet (UV) through the visible to infrared spectrum, is the preferred material system for inorganic LEDs.[21] Hybrid white light emission may generally be achieved using three primary colors (red, green, and blue) or two contrasting colors (blue and yellow or greenish-yellow).[35] The first method is most common due to its better color stability. Traditional white LEDs have a very low color rendering index (CRI) and correlated color temperature (CCT), as the three essential constituents in the white LED spectrum have not been appropriately mixed.[36] A promising approach to address this issue involves the use of a hybrid inorganic/organic LED architecture. This setup involves coating a commercially available InGaN inorganic LED (n-UV LED) with an organic material whose absorbance band matches the emission wavelength of the inorganic LED. This combination effectively converts the high-energy blue light from the inorganic LED into lower-energy yellow-red light from the organic material, resulting in high-quality white light.[13,37–39]

Stimulus-responsive optical materials are among the most important emitters. The phrase "acid protonation emission" refers to the tunable fluorescence produced by protonation or deprotonation, a powerful stimuli-responsive approach that involves a reversible color shift in fluorescence caused by acid.[40–42] As a result, materials exhibiting acid-sensitive fluorescence have garnered significant attention across various domains. Developing sensor devices to identify dangerous compounds in the environment has been a prominent field of study due to their growing significance for environmental protection, social security, and industrial safety in recent years. Using sensors to identify harmful gases has drawn a lot of interest. In this rapidly expanding world, one of the leading causes of the emission of harmful acid–base vapors is the rapid expansion of agriculture and industry. These toxic fumes irritate the skin, eyes, and respiratory tract, threatening human health and the environment. In particular, ammonia poisoning poses a severe risk to the central nervous system of humans. The luminescence switching of organic fluorophores (HCl and NH_3 vapors) is one of the best methods for visually identifying dangerous gases.[43–45]

In many scientific fields, visualizing latent fingerprints (LFPs) is a crucial technical endeavor offering concrete evidence. Information encryption, forensic sciences, and medical diagnostics are fields that have shown great interest in fingerprints because of their complex patterns and chemical insights. Ridge patterns, minute minutiae, finer structures like pores, and particular edge characteristics are all examples of the comprehensive information encoded in fingerprints.[46] The suitability of a wide range of luminous materials, including both organic and inorganic chemicals, for LFP detection is examined. Organic compounds are exciting because they show high luminescence performance, flexible architectures, and low toxicity. However, especially at higher concentrations, their efficacy in LFP fluorescence imaging is limited by the problem of aggregation-caused quenching (ACQ). Aggregation-induced emission (AIE)-active organic compounds that show strong emissions in aggregated forms, such as solids or aqueous

solutions, are a recent trend.[47–49] As compared to traditional powder techniques, they have several advantages, including increased sensitivity, better visibility, compatibility with digital imaging, and multi-wavelength imaging. They are able to function on a wider range of surfaces, including greasy, oily, and weather-damaged surfaces. Fluorophores are essential for forensic experts because of these advantages, particularly when working with complicated surfaces or when high-definition imaging is required.[50]

For next-generation lighting and sensing technologies, fluorophores with high quantum efficiency, robust stability, and adjustable emission are needed. However, the solid-state aggregation-caused quenching (ACQ) that conventional fluorophores frequently experience restricts their applications in solid-phase devices. Also, traditional AIE fluorophores glow weakly or not in diluted solutions due to intramolecular motion and non-radiative transition. Dual-state emissive fluorophores overcome the conventional AIE constraint (low solution-state emission) by exhibiting high emission in both the aggregated/solid state and solution.[51–53] One of the greatest ways to get around this is to combine the advantages of hybridized localized and charge transfer (HLCT) and aggregation-induced emission (AIE) with dual-state emission (DSE), each of which has special benefits for optoelectronic applications. AIE-active compounds with DSE show good emission in solution and become extremely emissive during aggregation, unlike ordinary fluorophores that undergo ACQ.[54–56] Decreased intramolecular motion (RIM) and rigid conformation, which inhibit non-radiative decay routes, are responsible for this behavior. Because of their superior solid-state luminescence and environmental durability, AIE fluorophores have found effective applications in LEDs, sensors, and biological imaging. By combining charge transfer (CT) and localized excited (LE) states, HLCT fluorophores enable rapid radiative decay while using triplet excitons for increased efficiency. In addition to providing a practical solution to the ACQ problem faced by traditional emitters, they have enormous potential for use in fluorescent sensors, chemical detection, optoelectronic devices, biological imaging, LED manufacture, and other domains. Therefore, a fluorophore that combines the processes of AIE and HLCT may provide dual-state emission (DSE) and enhanced exciton utilization, making it extremely useful for real-world applications. D–π–A molecules with balanced LE and CT states and twisted conformation promote HLCT and AIE in the same molecule. Therefore, combining the HLCT feature with AIE characteristics is a positive way to achieve a win-win scenario. In this regard, here three imidazole-based D–π–A molecules with dual-state fluorescence properties have been developed and synthesized. Fig. 1 shows the design strategies of the fluorophores. The chemical structures are shown in Fig. 2. The synthesized fluorophores are employed as organic downconverter materials to fabricate hybrid white LEDs, pH sensors, and acid–base vapor sensors, and they are also used in anticounterfeiting applications.

Materials design strategies

As mentioned above, BI can act as both a donor and an acceptor depending on the connectivity; when it is connected with the strong electron-withdrawing group, it acts as a donor, and when it is connected with a strong electron-donating group, it acts as an acceptor. Due to this bipolar nature, the emission color can be tuned from blue to green by different connectivities. As previously reported by our group, when benzilimidazole is connected with tetrahydrodibenzophenanthridine it acts as a donor with deep-blue emission.[8] Therefore, in this work, to explore the role of benzilimidazole (as a donor or an acceptor) and its impact on the ICT emission behaviour, three D–π–A

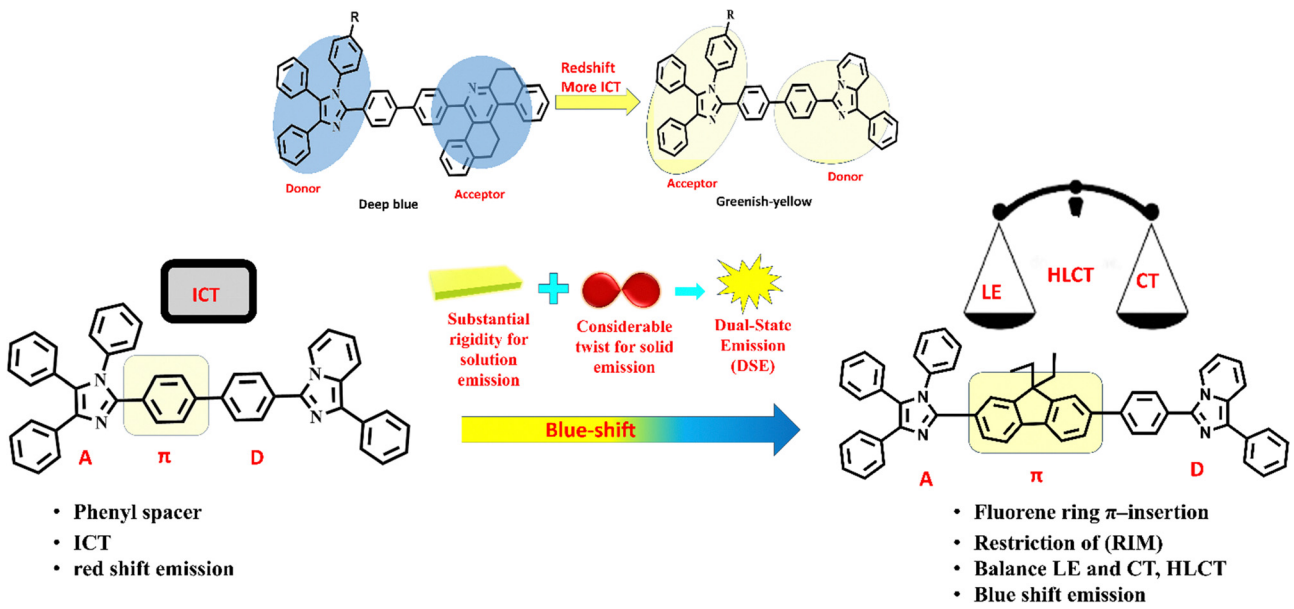

Fig. 1 Design strategies of the fluorophores.

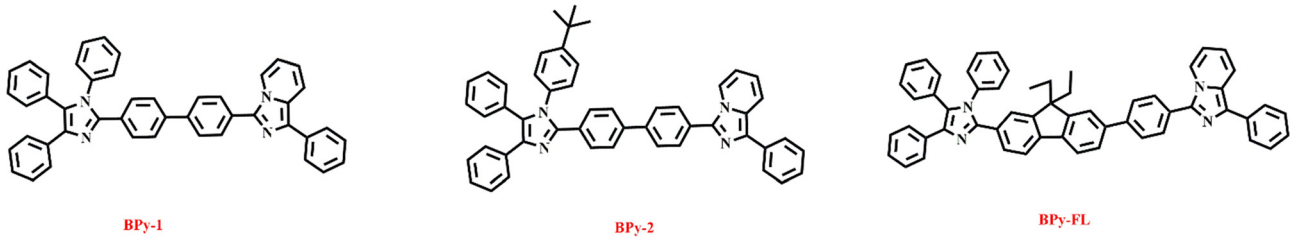

Fig. 2 Chemical structures of the synthesized fluorophores.

fluorophores are developed and synthesized by modifying the benzilimidazole core and connecting it with 1,3-diphenylimidazo[1,5-*a*]pyridine using different π-linkers (Fig. 2). In these synthesised fluorophores, when BI is connected with 1,3-diphenylimidazo[1,5-*a*]pyridine, it is found to act as an electron acceptor. It is also found to have enhanced delocalization of π-electrons and increased HOMO–LUMO overlap, responsible for the shift of the emission color to the yellow region with greater ICT. Hence, in this work, the N1 position of the BI ring is substituted with the phenyl ring and *tert*-butyl phenyl ring. The phenyl ring extends the conjugation and increases the ICT. The *tert*-butyl group is characterized by its considerable size and bulkiness, which increase steric hindrance. The large *tert*-butyl group makes the fluorophore more soluble and hydrophobic in organic solvents. By producing steric hindrance, the *tert*-butyl group lessens quenching caused by aggregation and stops excessive π–π stacking. As a result, solid-state lighting benefits greatly from improved solid-state fluorescence quantum yield. The *tert*-butyl group increases the thermal stability and photoluminescence quantum yield of the fluorophores. The absorption and emission spectra of the *tert*-butyl-substituted fluorophore are slightly blue-shifted as compared to the unsubstituted phenyl. This phenomenon may significantly influence the molecular conformation of the benzilimidazole derivative, thereby potentially modifying the rigidity and planarity of the molecular structure. **BPy-1** and **BPy-2** are synthesized using a phenyl π-linker between D and A units. The arrangement of the electron donor and acceptor groups at both ends of an aromatic π-bridge provides an electrical push–pull configuration that facilitates effective intramolecular charge transfer (ICT), as seen in Fig. 1.

Again, to determine the effect of the π-spacer, the fluorophore **BPy-FL** is synthesized, where the flexible phenyl group is replaced with a rigid and sterically hindered 9,9-diethyl-9*H*-fluorene ring in the π-bridge in the D–A framework. It is well known that the fluorene ring provides a high fluorescence quantum yield and a well-defined conjugation route by reducing the conformational flexibility in the D–π–A structure.[6,57] The close π–π stacking interactions between adjacent molecules are reduced by the steric bulk introduced by the diethyl groups at the 9-position of the fluorene ring, which may also promote the DSE properties.[58–60] When the fluorophore exhibits lower intramolecular mobility in the aggregated form, it is possible to get high fluorescence emission in the solid state. Furthermore, excessive twisting in the D–A fluorophore can lower emission efficiency, especially in the solution phase, which can be avoided with the insertion of a rigid core. The balance between LE and CT states in the rigid **BPy-FL** core, which is essential for HLCT behavior, is guaranteed by a moderate D–A interaction by introducing the 9,9-diethyl-9*H*-fluorene ring.

Three bipolar D–π–A emitters, **BPy-1**, **BPy-2** and **BPy-FL** (Fig. 2), are synthesized by combining the substituted benzilimidazole ring with 1,3-diphenylimidazo[1,5-*a*]pyridine (Scheme 1). Spectroscopic methods such as mass spectrometry and NMR spectroscopy were used to analyze the structural properties of the synthesized fluorophores. The electrical characteristics, thermal stability, and photophysical characteristics were thoroughly examined. The potential of these synthesized fluorophores as emitting molecules for the fabrication of white LEDs, pH sensors, and acid–base vapor sensors and for LFP detection and anticounterfeiting applications is explored.

Experimental section

Materials

All the reactions were conducted under a nitrogen atmosphere. The starting materials were purchased from a commercially available source (Sigma Aldrich) and used without further purification. The reactions were monitored by thin-layer chromatography (TLC) using silica gel 60 F_{254} aluminum plates (Merck). The silica gel (Sigma-Aldrich) was used for column chromatography.

Synthetic route

Using the Suzuki cross-coupling approach, the fluorophores **BPy-1**, **BPy-2** and **BPy-FL** are synthesized by mixing 3-(4-bromophenyl)-1-phenylimidazo[1,5-*a*]pyridine with 1,4,5-triphenyl-2-(4-(4,4,5,5-tetramethyl-1,3,2-dioxaborolan-2-yl)phenyl)-1*H*-imidazole, 1-(4-(*tert*-butyl)phenyl)-4,5-diphenyl-2-(4-(4,4,5,5-tetramethyl-1,3,2-dioxaborolan-2-yl)phenyl)-1*H*-imidazole and 2-(9,9-diethyl-7-(4,4,5,5-tetramethyl-1,3,2-dioxaborolan-2-yl)-9H-fluoren-2-yl)-1,4,5-triphenyl-1*H*-imidazole respectively (Scheme 1). Details of synthetic procedures of the fluorophores are mentioned in the ESI† (Sections S1 and S2). All the NMR and HRMS spectra are shown in the ESI† (S3 and S4). Intermediate **4** was synthesized by condensation between diketone, aniline derivatives, and aldehyde derivatives in the presence of ammonium acetate (NH_4OAc) and acetic acid (AcOH), as reported by our group previously.[61,62] The Miyaura borylation reaction was adopted to synthesize

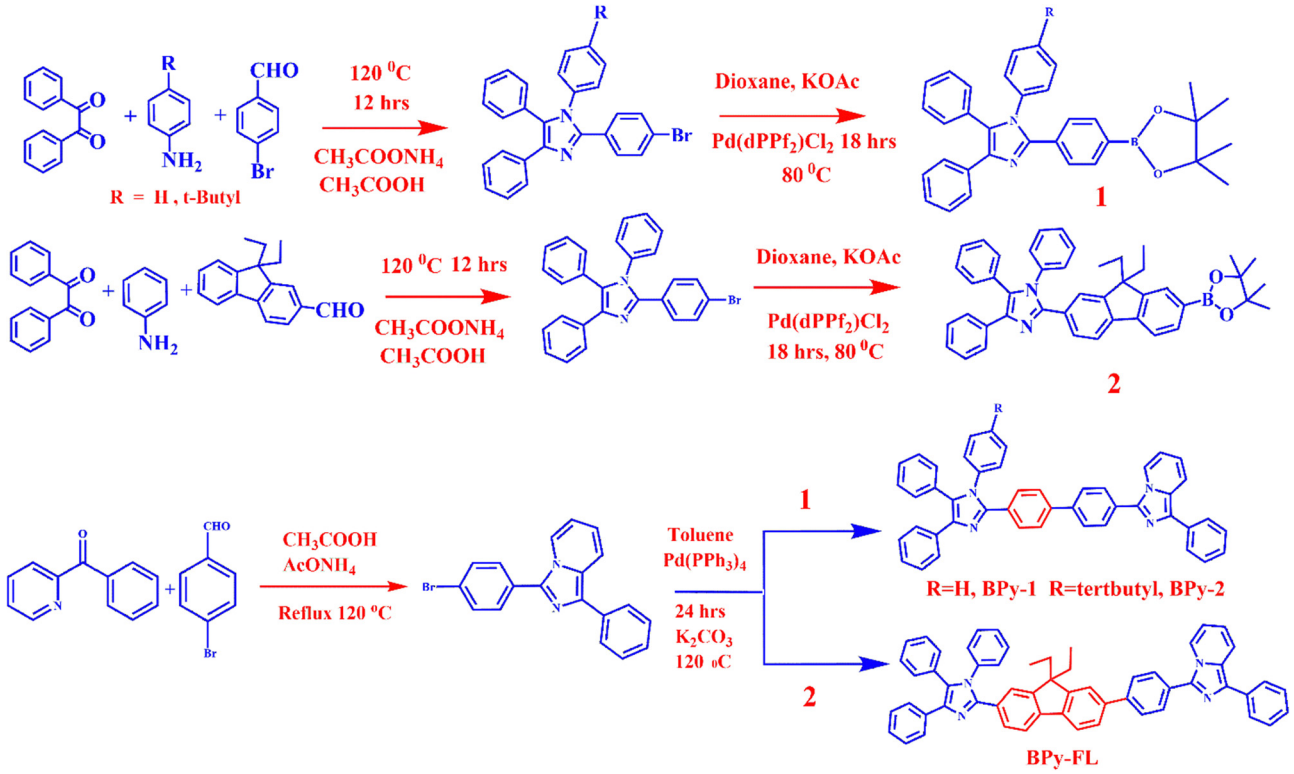

Scheme 1 Synthetic route of the fluorophores.

intermediates **1** and **2**. The Suzuki coupling reaction was used to synthesize the final products.

Results and discussion

Computational study

To comprehend the electrical properties and structural composition of fluorophores, density functional theory (DFT) and time-dependent DFT (TD-DFT) analyses were conducted using the B3LYP/6-31G(d,p) basis set.[63] Fig. 3 displays the geometries of the ground state, frontier molecular orbitals (highest occupied molecular orbital (HOMO)/lowest unoccupied molecular orbital (LUMO)), and the electrostatic potential map (ESP) of the fluorophores. The optimized geometry shows a rigid twisted structure. The dihedral angle (θ) between the imidazole and phenyl units in the optimized geometry is 53° and 54° for **BPy-1** and **BPy-2**, respectively. The angle between the phenyl spacer and the donor unit is 57° and 59° for **BPy-1** and **BPy-2**, respectively. **BPy-2** has a more twisted geometry than **BPy-1** due to the *tert*-butyl group at the N1 position, which slightly restricts the conjugation and breaks the planarity of the molecule as compared to the phenyl ring. In the case of **BPy-FL**, the dihedral angle between the acceptor unit and the fluorene ring is 64°, while the angle between the donor unit and the fluorene ring is 72°. This constrained molecular geometry is proposed to minimize energy loss during the non-radiative transition and aggregation-caused quenching by limiting intermolecular interactions.[64,65] From the electronic distributions, it is seen that the HOMO is mainly dispersed over the 1,3-diphenylimidazo[1,5-*a*]pyridine unit in all three fluorophores. The electron density of the LUMO is found to spread mostly across the π-bridge, phenyl ring of the [1,5-*a*]pyridine ring, and very tiny areas of the imidazole ring for **BPy-1** and **BPy-2**. **BPy-1** has a slightly greater HOMO–LUMO overlap as compared to **BPy-2** due to the phenyl ring at the N1 position, which extends the conjugation. This overlap of the HOMO and LUMO increases the charge transfer in excited states in both the fluorophores. In the case of **BPy-FL**, the HOMO is mainly localized in 1,3-diphenylimidazo[1,5-*a*]pyridine and the LUMO is located in the π-spacer fluorene ring and slightly extended up to the imidazole unit. Here the HOMO is mainly localized on the donor, whereas the LUMO is localized on the fluorene bridge and somewhat extended up to the acceptor imidazole unit. This partial separation of the HOMO and the LUMO reduces the energy gap between singlet and triplet energy levels and facilitates reverse inter-system crossing (RISC) from triplet to singlet states and also it balances the LE and CT characters, forming a hybrid HLCT excited state.[66,67] HLCT characteristics are confirmed using TDDFT. Singlet–triplet energy levels are calculated using TDDFT, and as seen in Fig. S11 (ESI†), the energy difference (ΔE_{ST}) between T_4 T_5 and S_1 is 0.07 eV. RISC occurs from the higher triplet state (T = 4,5) to the low-lying singlet state (S = 1,2) due to the small ΔE_{ST} between these states. This energy difference facilitates the hot exciton channel from the high-lying triplet state to the low-lying singlet state and can utilize the dark triplet exciton as radiative emission. For **BPy-1**, **BPy-2**, and **BPy-FL**, the expected HOMO/LUMO energies are

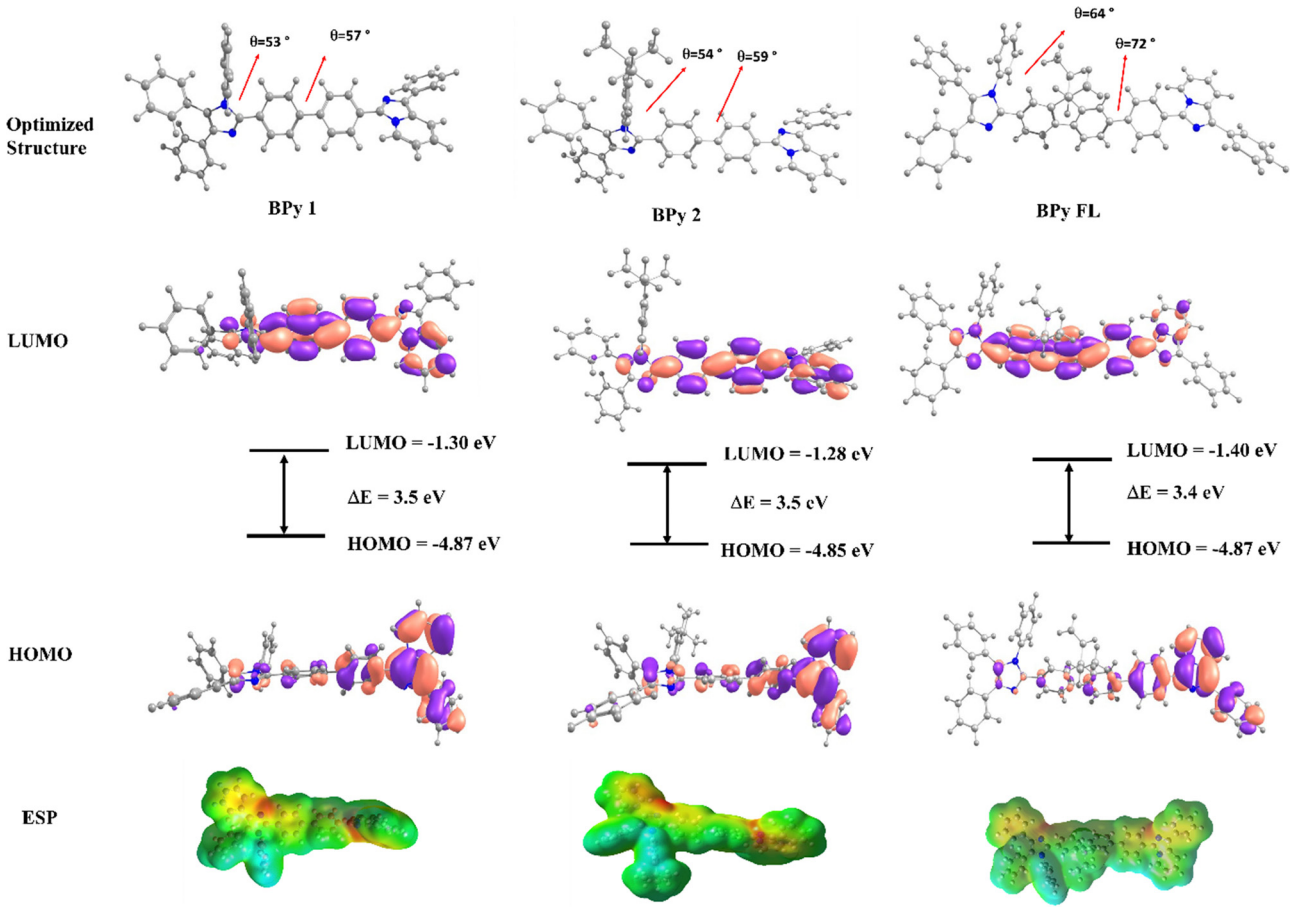

Fig. 3 Optimized molecular geometry, HOMO/LUMO energy levels, and electrostatic potential map of the fluorophores of **BPy-1**, **BPy-2** and **BPy-FL**.

−4.87/−1.30 eV, −4.85/−1.28 eV, and −4.87/−1.40 eV, respectively. The theoretical band gaps (E_g) of the fluorophores are found to be 3.5 eV for **BPy-1** and **BPy-2** and 3.4 eV for **BPy-FL**. The spread of ground-state electronic clouds was also examined using an ESP map. The highest negative potential (red cloud) for all the fluorophores is located in the pyridine ring nitrogen atom (–N=) and the imidazole nitrogen. In contrast, the phenyl rings of the benzylimidazole ring and the π-bridges have the highest positive potential (blue cloud). The green and yellow areas on the ESP map represent the neutral electrostatic potential of the fluorophores. Additional information, such as the atomic coordinates, singlet–triplet energy levels, oscillator strengths (f), and vertical transitions, is provided in the ESI† (SI6).

Thermal and electrochemical properties

To look into the thermal characteristics of the compounds, thermogravimetric analysis (TGA) and differential scanning calorimetry (DSC) were carried out in the nitrogen environment as shown in Fig. 4a. The DSC-TGA measurements were conducted between 30 and 600 °C at a scanning rate of 10 °C min^{-1}. All the fluorophores have high decomposition temperatures (T_d, or 5% weight loss), demonstrating good thermal stability. According to the DSC profile, no glass transition temperatures were found, and the fluorophores have remarkably high melting points (T_m) that match the melting point temperatures. Among these, **BPy-FL** has high T_d and T_m, *i.e.* 451 and 326 °C respectively. This may be due to the rigid structure and extended fluorene ring with the diethyl group. The T_d and T_m of the fluorophores are tabulated in Table 1. The HOMO/LUMO levels of the compounds were determined by cyclic voltammetry (CV) (Fig. 4b), which was performed using 0.1 M tetrabutylammonium perchlorate (Bu_4NClO_4) as an electrolyte support in DMF solvent at a scanning rate of 100 mV s^{-1}. It exhibits various oxidation and reduction activities and has the capacity to carry a bipolar carrier in the case of all the fluorophores. Based on the onset potentials, the HOMO and LUMO energy levels were calculated using eqn (1) and (2) by de Leeuw *et al.* The calculated HOMO and LUMO energy levels and bandgaps are tabulated in Table 1.

$$E_{HOMO} = -(E_{ox}^{onset} + 4.4)\ \text{eV} \quad (1)$$

$$E_{LUMO} = -(E_{red}^{onset} + 4.4)\ \text{eV} \quad (2)$$

Photophysical properties

The photophysical characteristics were examined using UV-vis and photoluminescence (PL) spectroscopy to understand the ground state and excited state properties of the fluorophores (Fig. 5).

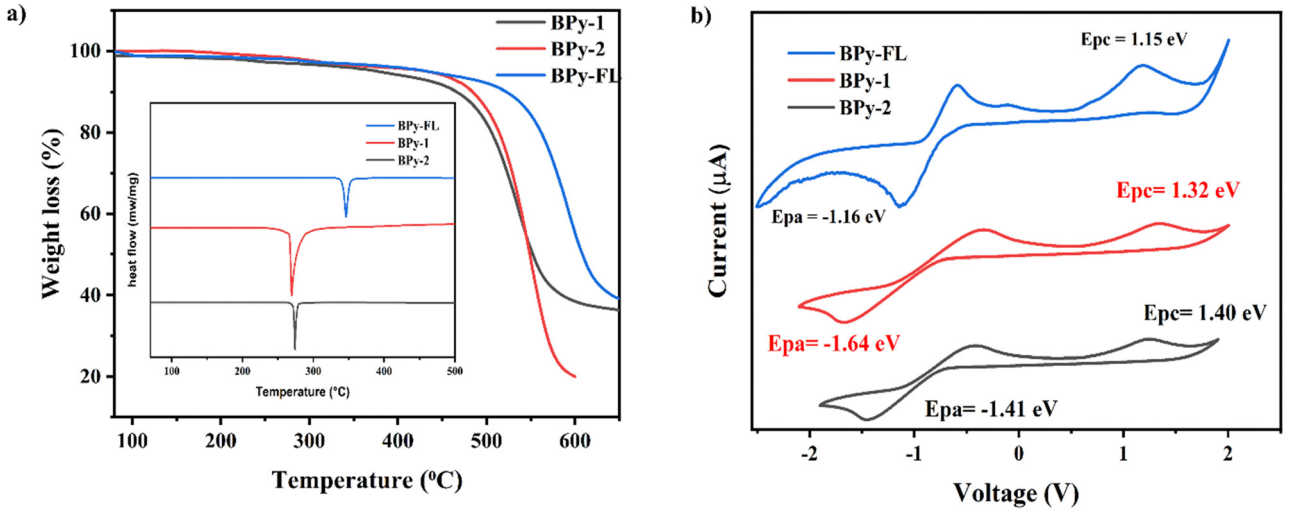

Fig. 4 (a) TGA and DSC curves of the fluorophores under the nitrogen atmosphere and (b) cyclic voltammetry (CV) of the fluorophores.

Table 1 Electrochemical and thermal properties of the fluorophores

Fluorophores	Thermal decomposition temperature (T_d)	Melting temperature (T_m)	HOMO (eV)	LUMO (eV)	Bandgap (E_g)
BPy-1	403.4 °C	269 °C	−5.61	−3.19	2.85
BPy-2	413.7 °C	270 °C	−5.62	−3.13	2.89
BPy-FL	451 °C	326 °C	−5.57	−3.28	2.29

The UV-vis spectra (10^{-5} M in toluene) show that all three fluorophores have almost identical absorption peak positions due to the structural similarities, as shown in Fig. 5a. The strong and intense peaks at around 255 nm are due to the localized π–π* transitions in the conjugated aromatic rings. Meanwhile, the intramolecular charge transfer from the donor to the acceptor is accountable for the lower energy higher wavelength absorption peaks at ∼365 nm. Diffuse reflectance spectra (DRS) (Fig. 5b) are used to calculate the optical band gaps using the Kubelka–Munk function.[68] The optical band gaps are determined to be nearly between 2.9 and 3 eV for all the fluorophores. The PL spectra (Fig. 5c) showed greenish-yellow emission for **BPy-1** and **BPy-2** and blue emission for **BPy-FL** in THF solutions (10^{-5} M) with maxima at 518 nm, 519 nm, and 464 nm, respectively. Due to the intermolecular interaction, the thin film and solid PL spectra (Fig. 5d) were redshifted to nearly 525 nm and 540 nm for **BPy-1** and **BPy-2**, respectively.[10,69] The fluorophore **BPy-FL** showed a highly intense emission peak at 509 nm in the solid state, as shown in Fig. 5d. **BPy-FL** exhibited dual-state emission in both solution and solid-states with different emission colors. The capacity of the fluorophore to show strong fluorescence in both the dissolved state of the solution and the aggregate/crystalline state of the solid with different emission colors is known as dual-state emission or DSE. This phenomenon is especially interesting since many conventional fluorophores experience ACQ in the solid state, where fluorescence quenching is driven by intermolecular interactions (such as π–π stacking). Here, all the synthesized fluorophores exhibit DSE characteristics, but the intensity of the solid-state emission is much brighter than the solution state for **BPy-FL**. It showed a bright greenish-yellow emission in the solid state. **BPy-FL** may exhibit Twisted Intramolecular Charge Transfer (TICT) effects in the solid state, in which redshifted fluorescence results from twisted conformations forming lower-energy emissive states. This may be due to the 9,9-diethyl-9*H*-fluorene ring. The phenyl ring is more planar than the substituted fluorene ring. So, the latter restricts and twists the conformation of **BPy-FL** as compared to the other two fluorophores. Due to the more twisted and rigid geometry, the conjugation is hampered in the case of **BPy-FL**. So the fluorophore **BPy-FL** exhibited blue shifted emission compared to the others. Fig. 9 shows the digital images of the fluorophores in thin film, powder form, and solutions under UV light (365 nm).

Aggregation induced emission (AIE) properties

Encouraged by the outstanding photophysical characteristics and intense emission in the solid state of the fluorophore **BPy-FL**, the aggregation-induced emission characteristics were examined in THF/H_2O mixtures with varying water percentages ranging from 0% to 99%. The AIE behavior of **BPy-FL** was examined by monitoring the variations in fluorescence intensity and UV-vis absorbance with the water ratio in a THF–water solvent mixture where THF functions as a good solvent and water as a non-solvent. Fig. 6 displays the UV-vis absorption and PL emission spectra of **BPy-FL** in THF with the gradual addition of water. The UV-vis absorption and fluorescence spectra in THF:water mixtures with different water fractions (F_w) were investigated while maintaining a constant **BPy-FL** concentration of 1×10^{-5} M. In pure THF medium, **BPy-FL** showed charge transfer absorption bands at a λ_{max} of 365 nm.

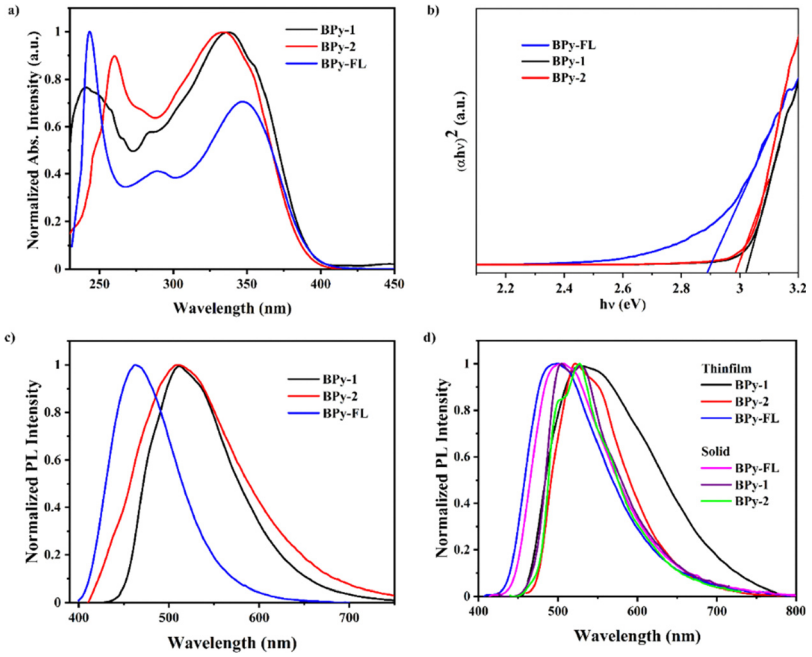

Fig. 5 (a) UV-vis spectra in dilute toluene solution (10^{-5} M); (b) diffuse reflectance spectra (DRS) measured using solid compounds; (c) PL spectra in THF (10^{-5} M); and (d) thin film and solid PL.

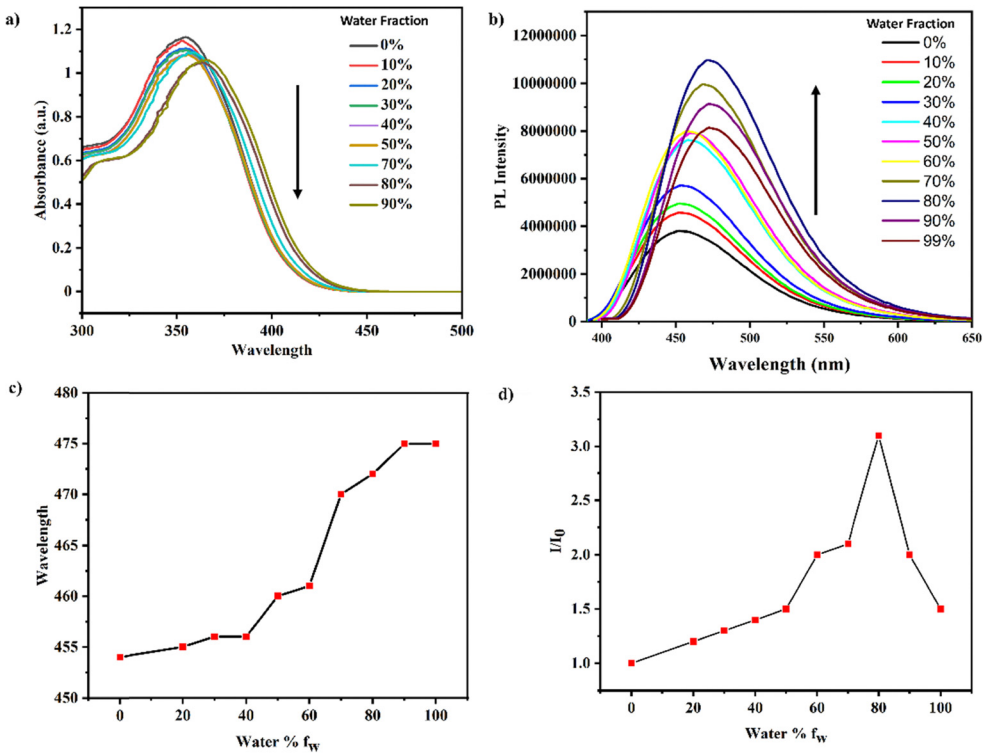

Fig. 6 (a) UV-vis absorption spectra; (b) fluorescence spectra of **BPy-FL** in different THF:water fraction (10^{-5} M) solutions; (c) plot of PL wavelength *vs.* water fraction; and (d) plot of PL intensity *vs.* water fraction.

Due to a higher level of the ICT effect in response to the increased solvent polarity of the THF:water binary combination, a bathochromic shift has occurred with an increased water volume fraction (Fig. 6a). The absorption maximum moved from 365 nm to 377 nm. It was discovered that absorbance gradually decreased when the water component increased to 80%, which

might be interpreted as a sign of aggregation development. **BPy-FL** showed poor solubility in water but great solubility in THF. It showed good blue fluorescence in THF when exposed to UV light (365 nm), but the fluorescence intensity again increased with greenish-blue emission when greater water factions were present. Due to aggregate formation in a water-rich medium, the fluorescence intensity was significantly increased, reaching an emission maximum at 475 nm at an 80% water fraction. According to this result, **BPy-FL** showed excellent emission intensity in both solution and aggregate forms. The emission intensity increased after 30% water fraction; when the water component is 80%, it is at its highest. It was discovered that the fluorescence intensity has increased by 6 times. A sharp rise in emission intensity showed the AIE characteristics of the compound, as seen in Fig. 6b. The emission intensity increases due to the restricted intramolecular rotation and motion in aggregate form, which decreases the non-radiative transition. Molecular interactions within the probe ensemble prevent aromatic rings from rotating freely in the aggregated state, suppressing non-radiative excited-state energy changes. Fluorescence emission is significantly increased due to excited-state molecules being forced to return to the ground state *via* radiative pathways. When F_w was raised beyond 80%, the fluorescence intensity of **BPy-FL** in the THF:water combination decreased, as shown in Fig. 7b. Typical AIE fluorophores only exhibit fluorescence upon aggregation and are normally non-emissive in solution due to intramolecular movements that allow non-radiative decay, but the fluorophore **BPy-FL** shows preferentially good emission in both solution and solid/aggregated states; this is an uncommon and desired characteristic for use in a variety of optoelectronic applications. The plots of wavelength and relative intensity (I/I_0) as a function of water fraction for **BPy-FL** are displayed in Fig. 6c and d, where I and I_0 represent the fluorescence intensities with and without water in the THF:water mixtures. These plots illustrate the variations in bathochromic shift and fluorescence intensity enhancement of the systems.

The fluorescence lifetimes were investigated to understand better the characteristics of the fluorophores in their excited states. Time-correlated single photon counting (TCSPC) was used to assess excitation decay, using the appropriate laser diodes by matching the emission maxima of the fluorophores.[70] The decay curves are depicted in Fig. 7, and the fluorescence lifetime data are represented in Table 3. The lifetimes of the synthesized luminophores were calculated using eqn (3).[6,71]

$$(\tau) = I_0 + A_1 \exp\left(-\frac{t}{\tau}\right) \quad (3)$$

where t is the time in nanoseconds, τ is the exponential decay time, A_1 is the scalar amount obtained from the curve fitting, and I_0 is the offset value (I_0 = 0). The lifetimes of the fluorophores were determined and are tabulated in Table 3. **BPy-FL** has a higher lifetime in the solid state than in solution, which may be due to the AIE properties of the fluorophores and due to the rigid and restricted conjugation, which increases the duration of the excited state and reduces non-radiative relaxation.

An integrating sphere was used to determine the photoluminescence quantum yield (Φ) of the fluorophores (Fig. S10, ESI†). The quantum yield of all the fluorophores is mentioned in Table 2. The Φ of **BPy-2** is more than that of **BPy-1**, which may be attributed to the *tert*-butyl substitution, which restricts the rotational and vibrational motion and increases the radiative

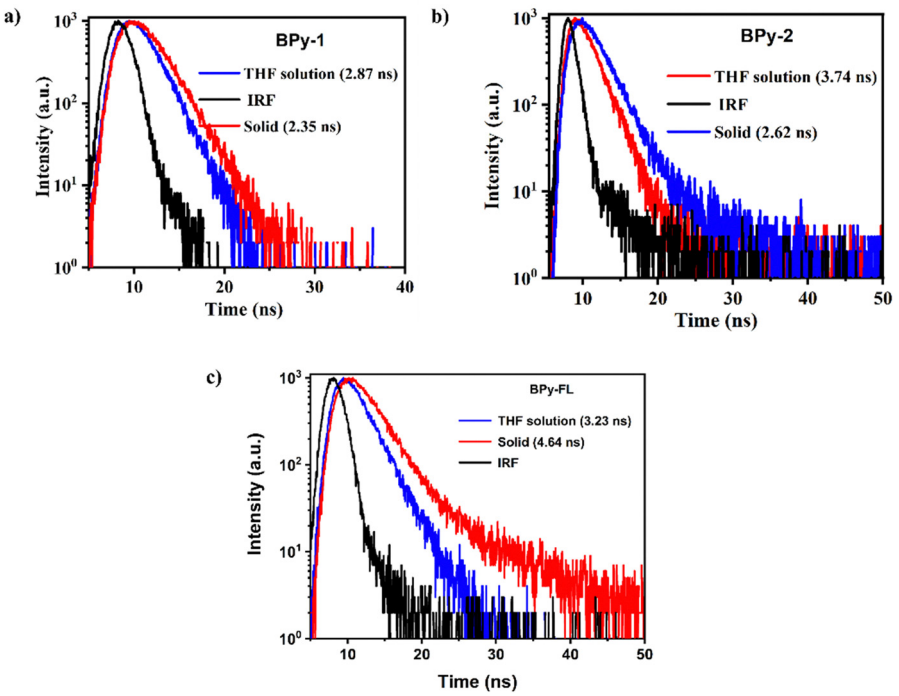

Fig. 7 Time-resolved PL decay of (a) **BPy-1**, (b) **BPy-2**, and (c) **BPy-FL**.

Table 2 Key photophysical data

Fluorophores	λ_{abs} (nm)	λ_{ems} (solution/thin film/solid) (nm)	Lifetimes (τ) in ns	Quantum yield (Φ)	k^r (10^7 s^{-1}) THF/solid	k^{nr} (10^7 s^{-1}) THF/solid
BPy-1	260, 370	521, 525, 535	2.87 (THF) 2.35 (solid)	53% (THF) 42% (solid)	18.4/17.8	20.3/16.2
BPy-2	255, 373	519, 530, 532	3.74 (THF) 2.62 (solid)	72% (THF) 47.3% (solid)	19.2/18	19/15.7
BPy-FL	268, 378	460, 508, 509	3.23 (THF) 4.64 (solid)	77.6% (THF) 93.6% (solid)	24/20	18.5/17.7

pathway as compared to simple phenyl substitution. **BPy-FL** has a maximum quantum yield of 77.6% in solution and 93.6% in the solid state among all the fluorophores. The higher quantum yield in the case of the solid state of **BPy-FL** is due to the reduction in non-radiative transition in the excited state due to minimized intermolecular interaction and AIE-HLCT behavior with DSE of the fluorophores.[70,71] Additional photophysical data on the fluorophores are mentioned in SI5 (ESI†). Additionally, their radiative rate (k^r) and non-radiative rate (k^{nr}) were determined using eqn (4) and (5), and the corresponding data are tabulated in Table 2. The k^r of **BPy-FL** is higher than that of other fluorophores. This may be due to its twisted geometry and HLCT-AIE characteristics. **BPy-2** has a lower k^{nr} and higher k^r than **BPy-1** due to the *tert*-butyl phenyl group, which decreases the nonradiative transition compared to the phenyl ring.

$$k^r = \Phi_F/\tau_F \quad (4)$$

$$k^{nr} = k^r/\Phi_F - k^r \quad (5)$$

Solvatochromism

Furthermore, to better understand the intramolecular charge transfer phenomena in excited states, solvatochromic studies were carried out, and the associated spectra are depicted in Fig. 8, while the corresponding data are presented in Tables ST1–ST3 and (SI5) (ESI†). From low-polar hexane to high-polar ACN, all the emitters exhibited distinct solvatochromic phenomena that can be readily observed from the fluorescence spectra. Fig. 8 displays the emission and absorption spectra in various solvents. Fig. 9 displays the digital images of the solvatochromic study. The absorption spectra in Fig. 8a showed little to no influence on the polarity of the solvent. On the other hand, it was clear from the emission spectra that the solvent polarity affected the emission peaks significantly, which were redshifted with increasing solvent polarity for all the fluorophores. This denotes a positive solvatochromism, and the ICT occurs when the molecule is excited. From low polarity solvent hexane to high polarity solvent ACN, there was a red shift of over ~90 nm for **BPy-1** and **BPy-2** and 85 nm for **BPy-FL**, respectively, in the PL spectra, shifting them to a longer wavelength. The full-width half maxima (FWHM) and PL emission peaks both expanded, providing a convincing explanation for the CT excited states in all the fluorophores. In the case of **BPy-FL**, structured vibrational peaks are observed in low polar solvents like hexane, toluene, and dioxane, and they become nonvibrational and widened in the case of high polar solvents; this indicates the combination of LE and CT states of the fluorophores. The LE state-dominated emission is shown by

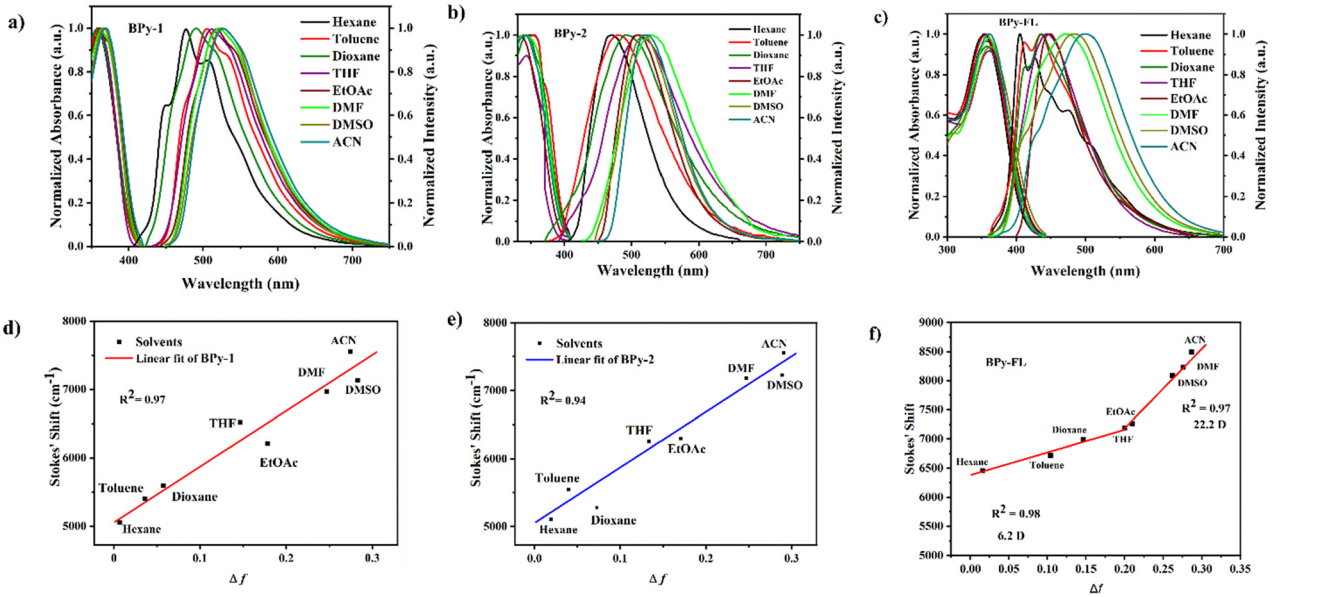

Fig. 8 Absorption and emission spectra of fluorophores in different solvents: (a) **BPy-1**, (b) **BPy-2** and (c) **BPy-FL** and Lippert–Mattaga plots of (d) **BPy-1**, (e) **BPy-2** and (f) **BPy-FL**.

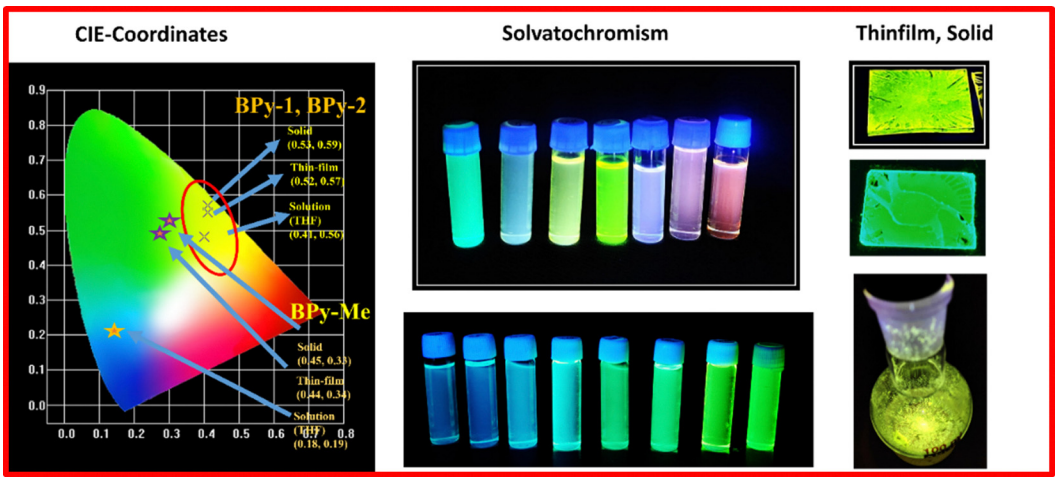

Fig. 9 CIE-coordinates of the fluorophores (solution, thin film, and solid), digital images of the fluorophores under UV-light (365 nm) in different solvents (nonpolar to polar), thin film and solid form.

BPy-FL in low polar solvents with clear shoulder peak emission (Fig. 8c). When the solvent polarity increases, the shoulder peak goes away, and the emission in high polarity acetonitrile rises to 512 nm with a red-shift of 85 nm, indicating the appearance of the CT state. The CT states of the molecule in the excited state are getting more stabilized in polar solvents. The emission color was shifted from blue to green from hexane to ACN in **BPy-FL**. The reasons for the longer wavelength shift in the emission spectra in the high polar solvent are (a) structural reorganization in the excited state and (b) photo-induced ICT stabilization in the polar solvent.[72–74] These variations in solvatochromism in emission spectra compared to absorption spectra suggested that the dipole moments of the fluorophores were greater in the excited state than in the ground state. Additionally, a progressive rise in Stokes shift was seen as solvent polarity increased, consistent with the Lippert-Mataga plot. Fig. 8(d–f) displays the Lippert–Mataga plot, which illustrates the relationship between solvents and the dipole moments of the solute in both the lowest excited state (S_1) and the ground state (S_0). The Lippert–Mataga plot displays the orientation polarizability (Δf) *versus* Stokes shift (ν_g–ν_e) in various solvents of the fluorophores. The orientation polarizability (Δf) and Stokes shift are directly proportional or have a straight-line connection for the fluorophores **BPy-1** and **BPy-2** as shown in Fig. 8(d) and (e), whereas the Lippert–Mataga plot of **BPy-FL** shows two straight lines (bilinear) (Fig. 8f): one is for low polar solvent (R^2 = 0.98) and another one is for high polar solvent (R^2 = 0.97). The plot of **BPy-FL** is separated into two separate sections, with CT dominating at high polarity and LE dominating at low polarity. The dipole moment of **BPy-FL** was calculated using the previously reported method.[75] In low polar solvent, the dipole moment was calculated as 10.2 D, and in high polar solvent, the dipole moment was found to be 22.2 D. This confirmed the combination of LE and CT (HLCT) excited states of **BPy-FL**. The Stokes shift and the Lippert–Mataga parameter are likewise shown to have a good association, with slopes of 1447 and 1534 and R^2 values of 0.97 and 0.94 for **BPy-1** and **BPy-2** respectively. The ground state dipole moments are found to be 6 D and 7.2 D for **BPy-1** and **BPy-2** respectively from the DFT study, and using the previously published equation, the excited state dipole moment was determined to be 16.2 D and 17.3 D for **BPy-1** and **BPy-2** respectively, based on the Lippert–Mataga plot.[17,76,77]

Fabrication of white LEDs

By taking advantage of the greenish-yellow emission of all the fluorophores, we have used the fluorophores as organic down converter materials to fabricate white LEDs. A three-component system is used to fabricate the white LEDs. To fabricate the white LEDs, the synthesized fluorophores are mixed with a red component (Eu(II) complex, previously reported by our group) and coated over widely available InGaN LED chips (390 nm) by taking into consideration a simple and environmentally friendly approach for applying the hybrid system in actual devices.[78] The fluorophores and the Eu complex were dissolved in the THF solvent. Then, PMMA (a suitable host material) was added to the solutions, and it was either embedded in a sol–gel matrix or cast onto a substrate. PMMA and the fluorophores are mixed in THF to create a gel-like substance at room temperature. A UV LED chip is coated with a luminescent layer (gel substance) to make hybrid white LEDs. The solvent and moisture from the LED chip were removed by spin coating. The spin coating technique involves spinning the LED at a controlled speed to coat it with a small amount of gel to generate an equal layer. White LEDs were fabricated by coating a blue LED with the synthesized fluorophores and the red organometallic phosphor (Eu(II) complex) in an appropriate mass ratio by a trial-and-error method. The ratio was optimized to produce LEDs with improved emission efficiency with warm white light (CRI > 85 and CIE in the range of 0.35,0.32). Excellent EL intensity and CRI values of the hybrid white LEDs were observed for the 2 : 1 ratio of the red phosphor and the synthesized fluorophores, which is superior to the other tested ratios. So, the white LEDs were fabricated by taking a 2 : 1 ratio of the red phosphors and

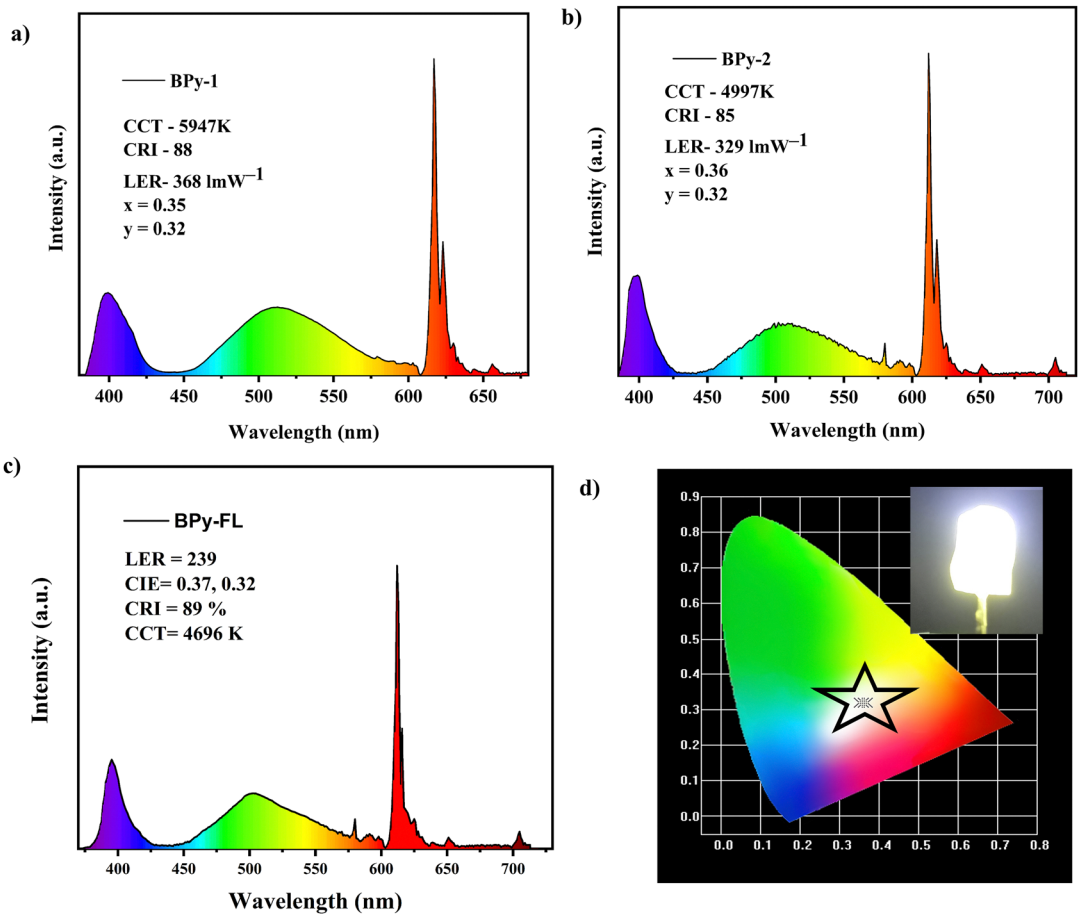

Fig. 10 PL spectra of the white LEDs fabricated using blue LED chips using the synthesized fluorophores and Eu complexes: (a) **BPy-1**, (b) **BPy-2**, and (c) **BPy-FL** and (d) CIE-coordinates of the fabricated white LEDs.

the synthesized fluorophores by mixing with PMMA in THF solvent and coating over a UV LED chip. PMMA was selected because of its favorable optical characteristics and low oxygen and moisture permeability, which prevent quenching processes and dopant dye oxidation. PMMA is frequently utilized in applications that need favorable mechanical, thermal, and chemical resilience and exceptional optical quality.[79] Fig. 10 displays the EL spectrum of the fabricated white LEDs. All the fluorophores show warm white light emissions with CRI values of more than 85 and a CIE coordinate of nearly (0.35,0.32), almost precisely aligned with the NTSC standard value of white light emission. Among all the fabricated white LEDs, **BPy-FL** showed the highest CRI value of 89. The digital images and CIE coordinates of all the fabricated white LEDs are displayed in Fig. 10, and the EL data are tabulated in Table 3.

Table 3 EL data of the fabricated white LEDs

Fluorophores	CCT (K)	CRI	CIE	LER (lm W^{-1})
BPy-1	5947	88	0.35, 0.32	368
BPy-2	4997	85	0.36, 0.32	329
BPy-FL	4696	89	0.37, 0.32	239

Acidochromism, vapoluminescence and anticounterfeiting

As mentioned earlier, in molecules with D–π–A push–pull framework, the ICT emission characteristics are highly dependent on donor ability, acceptor ability, and π-conjugation. In the present work, all the donor and acceptor units contain an amphoteric imidazole unit with a basic N-atom. It is anticipated that in an acidic environment, with the addition of H^+ ions, the donor and acceptor ability of the D–π–A unit will change upon protonation of the basic nitrogen. Therefore, a significant change in the emission characteristics of these fluorophores is expected, and these molecules are utilized as fluorescent pH sensors. Furthermore, as these fluorophores show strong emission in solid and thin film states, their potential as fluorescent vapor luminescent acid–base sensors and anticounterfeiting materials is also studied.

The imidazo[1,5-*a*]pyridine ring holds the majority of the HOMO, indicating that this area of the molecule has the higher nucleophilic (electron-rich) sites and is more reactive to protonation. Because, in this particular case, electronic and orbital parameters determine the precise location of protonation. The imidazo[1,5-*a*]pyridine nitrogen undergoes protonation to produce a conjugate acid stabilized by resonance in the fused heterocyclic system. So in an acidic environment, the nitrogen

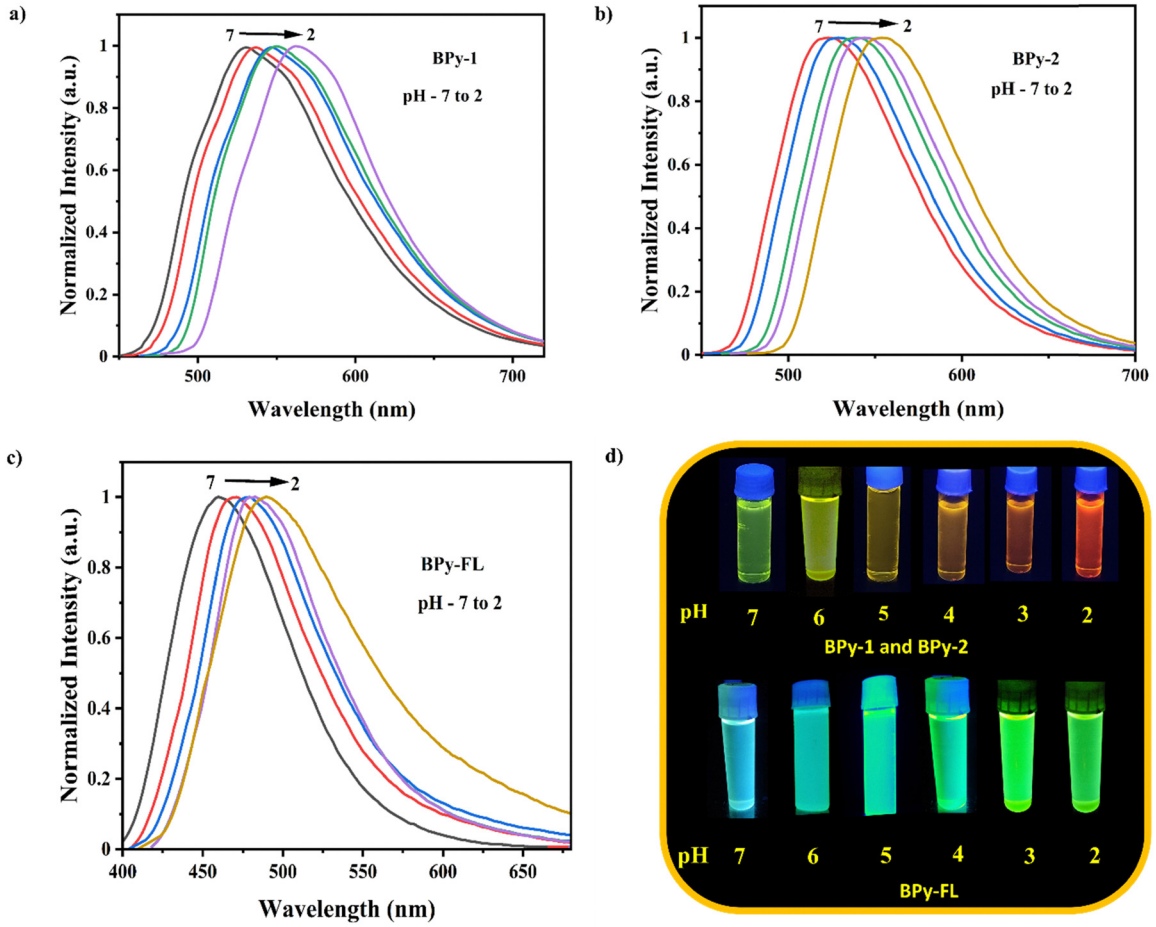

Fig. 11 Fluorescence spectra of fluorophores in THF solutions (1×10^{-5} M) at different pH values: (a) **BPy-1**, (b) **BPy-2** and (c) **BPy-FL**.

atom in the imidazo[1,5-*a*]pyridine ring can take up a proton. By protonation, the electronic structure of the molecule changed, and its photophysical characteristics also altered, ultimately causing the emission spectrum to redshift. The reversible color and emission shifts of the fluorophores in response to pH variations demonstrate their acidochromic characteristics. Fig. 11 displays the acidochromic behavior of the fluorophores in THF solutions. The digital image of these solutions under UV light at 365 nm (Fig. 13 and 14) demonstrates the excellent acidochromic behavior of these solutions by displaying a dramatic change in fluorescence color upon pH variation. In the pH range of 7 to 10 (neutral and higher), **BPy-1** and **BPy-2** appeared greenish-yellow. These solutions looked yellowish-orange when the pH decreased from 5 to 4, and they turned orange when the pH was reduced even lower than 3. In the case of **BPy-FL**, at neutral pH, it showed blue emission, but at higher pH, the emission color changed to green, as shown in Fig. 13c. It is evident from the discovery above that the synthesized fluorophores can be used as fluorescent pH sensors in the acidic pH range of 3–5, as they exist in different spectroscopically different protonated and neutral forms in this range. In Fig. 11, the different color appearances, a notable bathochromic shift in the PL spectrum from 510 to 560 nm (**BPy-1** and **BPy-2**) and 464 to 511 nm (**BPy-FL**), and a broadening of the fluorescence peak at lower pH suggested a more substantial intramolecular charge transfer because protonation had formed a stronger acceptor in the D–π–A molecule. Due to this, the HOMO LUMO of the fluorophores also altered. The CIE coordinates of the fluorophores in different pH media are mentioned in ESI,† SI7. Furthermore, triethylamine (TEA) and TFA were added alternately to the THF solution of fluorophores (Fig. 13) to examine the reversibility of the pH response characteristics of each of these probes. The emission maxima were observed to return to their starting state after adding 40 μL to 30 μL of triethylamine (TEA) to the fluorophores. It is possible to repeat this cycle multiple times without experiencing a noticeable reduction in the pH sensor ability of both the fluorophores. Since the procedure is non-destructive, the reversible transition could be carried out numerous times by switching the alternate addition of TFA and TEA. The CIE coordinates of the fluorophore **BPy-2** and the digital image of the fluorophore in THF solution with alternate addition of TFA and TEA are shown in Fig. 13.

^{1}H NMR titration studies of the molecules with different equivalents of TFA (0 and 2 equiv.) were conducted to investigate the change in the structural pattern with alternate addition

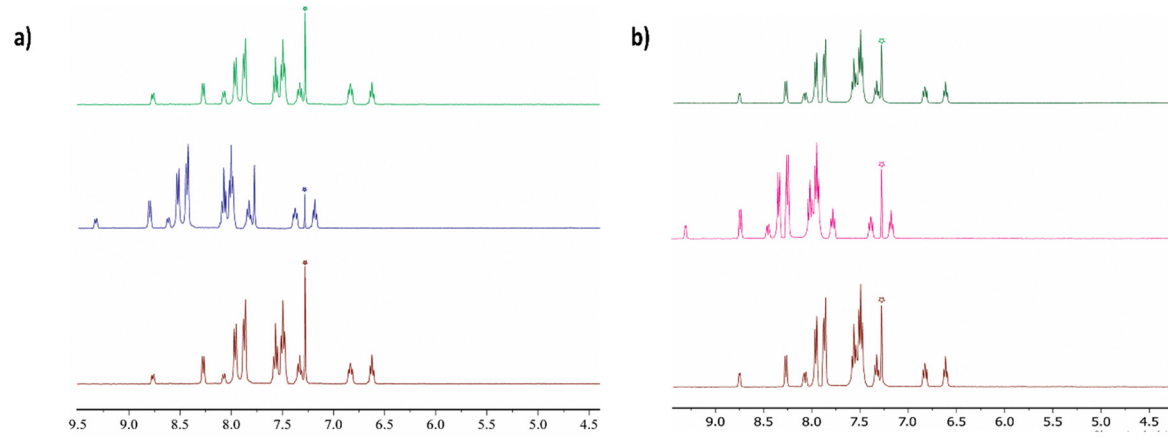

Fig. 12 ^{1}H NMR spectra of the fluorophores in $CDCl_3$ before the addition of TFA (lower spectra) and after the addition of 2 equiv. of TFA (middle) and 10 equiv. of TEA (upper): (a) **BPy-1** (b) **BPy-2**.

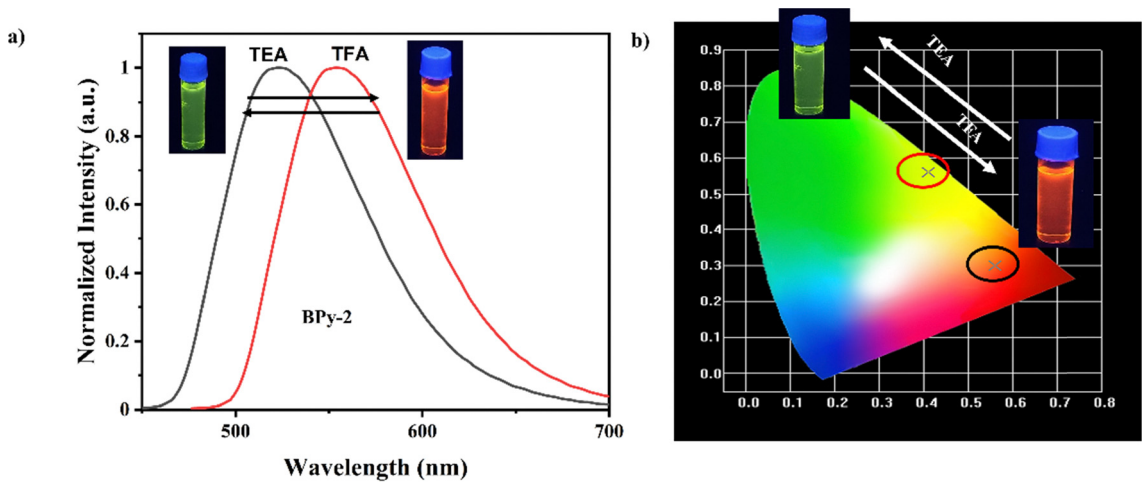

Fig. 13 (a) Fluorescence spectra of **BPy-2** with alternate addition of TFA and TEA; (b) digital images of the fluorophores at different pH values; (c) CIE-coordinates and digital images of the fluorophores with alternate addition of TFA and TEA.

of acid and base (Fig. 12 and Fig. S15, ESI†). TFA was demonstrated to cause a downfield shift in the chemical shifts for the phenyl protons and the aromatic protons in all molecules. This may be due to the formation of protonated species. Again, the ^{1}H NMR spectra are entirely restored by adding excess TEA to the solution, suggesting that the change in the protonated species is reversible and non-destructive.

Application on paper strips

Using the portable paper strip technique, test cellulose paper strips were coated with the probes (0.5×10^{-3} M) and then dipped in different pH solutions (pH of 7, 6, 5, 4, and 2) to investigate the practical use of fluorophores as pH sensors. All the fluorophore-coated test strips responded significantly to each pH solution in terms of color change, as shown in Fig. S14 (ESI†). The variations in fluorescence showed that simple test strips could detect acidic pH and that all the fluorophores had excellent pH selectivity.

To ascertain the changes in the electronic properties of the fluorophores and to better understand the protonation mechanism upon interaction with TFA, DFT analysis was carried out for **BPy-1**-H^+, **BPy-2**-H^+ and **BPy-FL**-H^+ (representing fluorophores after interaction with TFA) and compared with that of the electron cloud distribution of the front-line orbitals of **BPy-1**, **BPy-2** and **BPy-FL** (Fig. 14 and Fig. S12, S13, ESI†). Both the HOMO and LUMO energy levels were decreased significantly upon protonation with a reversal in electronic distribution. Just opposite to **BPy-1**, **BPy-2** and **BPy-FL** in the case of **BPy-1**-H^+, **BPy-2**-H^+ and **BPy-FL**-H^+ the HOMO is distributed in the benzilimidazole unit and the 1,3-diphenylimidazo[1,5-*a*]pyridine group contained the LUMO orbitals of fluorophores. After protonation, the band gaps of the fluorophores decreased and were found to be 2.28 eV, 1.75 eV, and 1.5 eV for **BPy-1**, **BPy-2**, and **BPy-FL**, respectively. Also, acid protonation decreases the overlap between the HOMO and LUMO of both the fluorophores. The HOMO and LUMO are entirely separated after protonation, due to which the CT state of the excited molecules is enhanced, and the emission peak in the PL spectra is redshifted.[80–82]

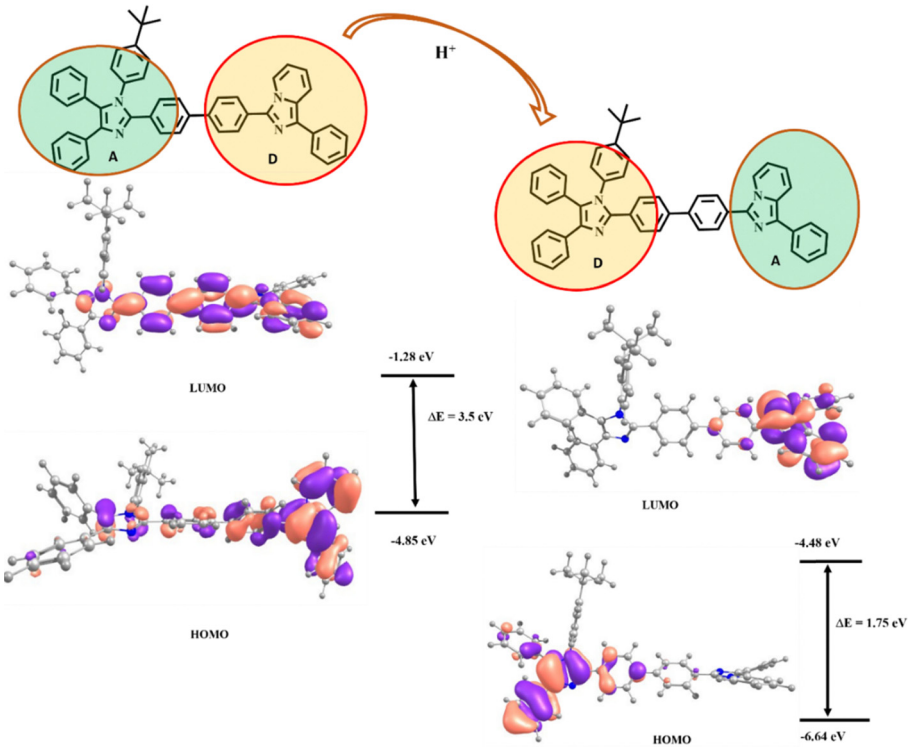

Fig. 14 HOMO–LUMO energy levels of **BPy-2** before protonation and after protonation.

The acid sensitivity of the emission features of the fluorophores is exploited for fluorescence vapoluminescence sensing applications. Numerous molecules for vapoluminescence applications have been reported so far, such as carbon dots, europium complexes, nanocomposites, luminous supramolecular compounds, compounds based on β-diketone-based Eu(III) complexes, and Eu(III) polymers.[14,37,83] To the best of our knowledge, very few small organic fluorophores are reported as vapor sensors. The vapoluminescence application was studied by taking the thin films of **BPy-1**, **BPy-2** and **BPy-FL**. The synthesized compounds in this investigation exhibit recyclable on–off–on vapoluminescence activity (Fig. 15 and Fig. S16, ESI†). The color variations, as indicated by the PL emission spectrum studies, are noteworthy, and Table ST17 (ESI†) lists the CIE color coordinates of the compounds subjected to acid–base vapors. The suitability of the synthesized fluorophores as vapoluminescent sensors was evaluated by looking at their PL emission in response to NH_3 and HCl vapors. The thin film of the compounds peaked at ~520 nm (**BPy-1** and **BPy-2**) and 495 nm (**BPy-FL**) before exposing to the HCl vapor, indicating green emission. After a few minutes of exposure to HCl vapor at room temperature, a rapid vapochromic behavior was observed, and the emission shifted to 561 nm (**BPy-1** and **BPy-2**) and 570 nm (**BPy-FL**). Under a UV lamp, the color of the films was changed from green to orange. Additionally, green emission was restored when NH_3 vapor was introduced into the thin film, leading to the "switching on" of a 520 nm and 495 nm peak. When imidazole-based fluorophores are subjected to acidic vapors, the imidazole basic nitrogen is protonated. This protonation changes the electronic structure of the fluorophore, which in turn changes the fluorescence properties.[37,84]

Information security is crucial in daily living, the economy, society, and the military. As a result, the creation of novel materials has drawn much attention due to their potential for applications in protection and counterfeiting detection. The successful investigation of vapor response characteristics of the fluorophores allowed us to determine their anticounterfeiting potential. The term "NIT RKL" was handwritten on clean filter paper using a brush pen loaded with a suspension of **BPy-1** in THF. The behavior of luminescence in the interaction with HCl and NH_3 vapor is shown in Fig. 15d. Images were captured using a UV light with a 365 nm wavelength. Images in Fig. 15d, taken under the UV light, show that the green emission returns when base vapor is passed through it. The second picture also shows how exposure to acid vapor causes the green emission to quench immediately.

Latent fingerprint application (LFP)

Obtaining fingerprints from crime scenes provides crucial information for identifying potential suspects. Generally speaking, latent fingerprints (LFPs) are difficult for the human eye to recognize. By taking advantage of the intense solid-state emission and AIE properties of **BPy-FL**, we have used it in LFP for anticounterfeiting applications. The development of LFPs is shown in Fig. 16. The finger of a person was thoroughly cleansed with cotton wipes. The finger was then pressed against various surfaces, such as glass and plastic, and cleaned using the fatty substances produced by the body.

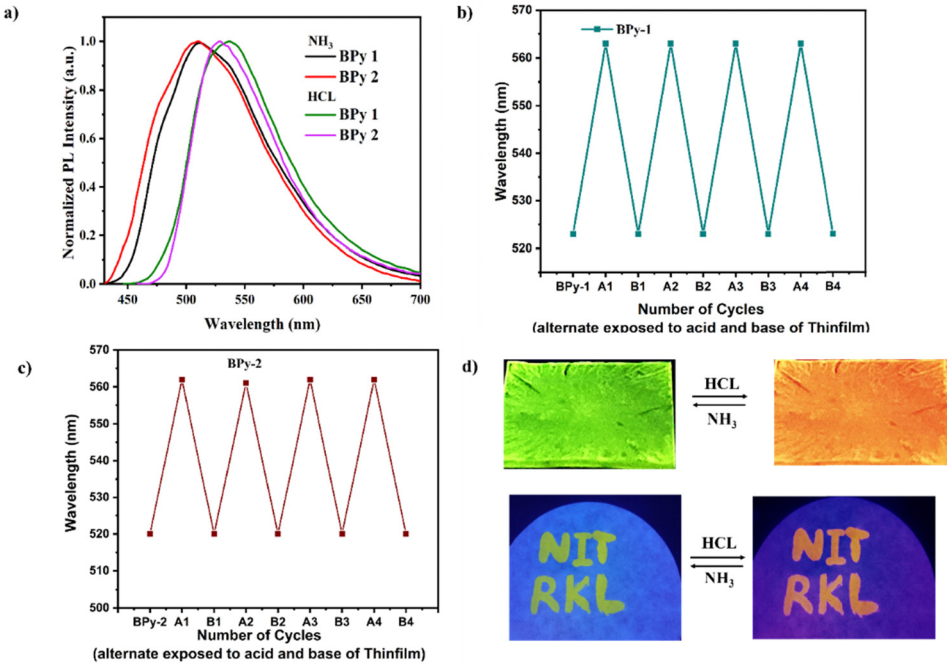

Fig. 15 (a) Thin-film PL spectra of the compounds upon exposure to acid–base vapors, (b) and (c) luminescence cycle of the fluorophores upon exposure to acid–base vapors, (d) luminescence pictures of thin-film and "NITRKL" was written on filter paper using a brush pen filled with a suspension of the fluorophores in the absence of vapors (under a 365 nm UV lamp), Restoration of the emission in the presence of NH_3 and quenching in the presence of HCl vapor.

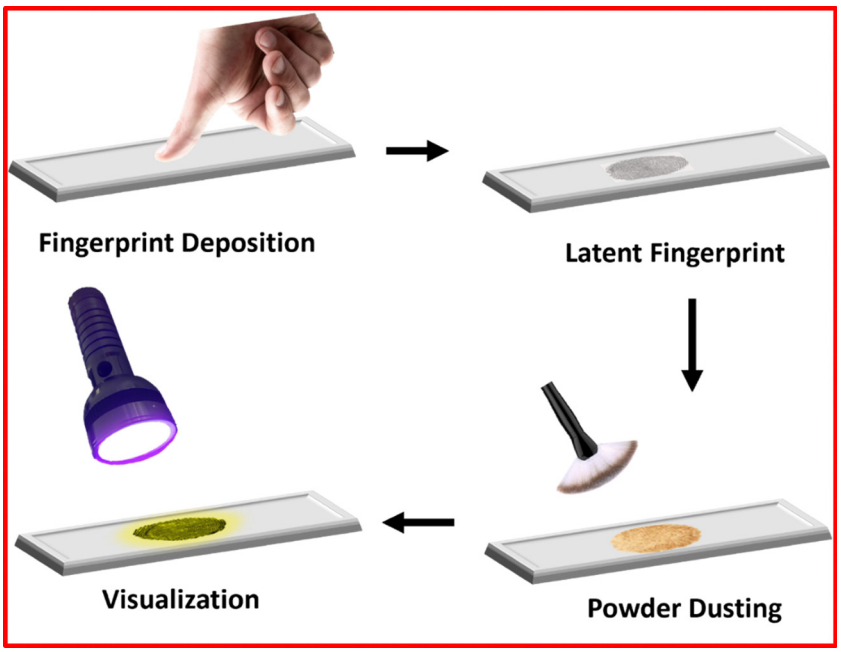

Fig. 16 Development of LFPs.

As seen in Fig. 17, the fingerprints are invisible until the compound **BPy-FL** is powdered and made brightly visible under UV light of 365 nm. Latent fingerprints leave behind oily residues that contain fatty acids, amino acids, and sebum when they come into contact with an object's surface. Using their desired properties, fluorescent powders of the synthesized materials were uniformly applied to various material surfaces using a brush. The distinct separation of the fingerprint layers makes them identifiable (Fig. 17). Characteristics of level 1 and level 2 fingerprints, such as loops (1), crossings (2), bifurcations (3),

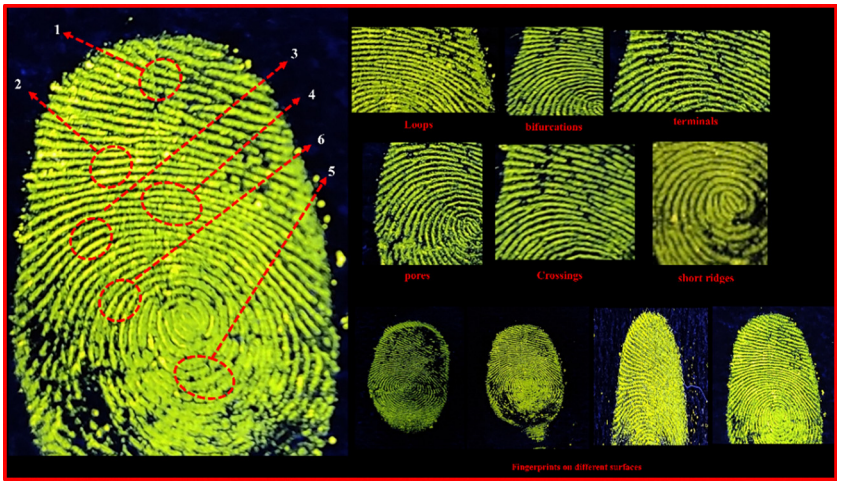

Fig. 17 LFP applications of **BPy-FL**.

terminals (4), and short ridges (5), as well as level 3 characteristics, including pores (6), are clearly visible in enlarged photos (Fig. 17).

This demonstrates that using **BPy-FL** for latent fingerprints can be advantageous. LFPs were positioned on the glass slide surface and left there for 2, 10, 20 and 30 days without coming into contact with anything throughout the deposition process to test the repeatability of fingerprints using this technique. The aged LFPs were then stained with the fluorophore and photographed under 365 nm UV light. Clear identification of all these aged fingerprints as bright fluorescent images clearly demonstrated the feasibility of BPl-Fl in fingerprint detection.

Conclusion

In conclusion, we present a systematic report on the design, synthesis and versatile applications of three D–π–A based push–pull fluorophores (**BPy-1**, **BPy-2**, and **BPy-FL**) featuring N1-substituted imidazole and imidazo[1,5-*a*]pyridine D–A conjugates attached through flexible phenyl or rigid and sterically hindered diethylfluorene as the π-conjugated spacer unit. The role of spacer units in modulating their photophysical properties especially the emission wavelength and quantum yield has been analyzed and explained through DFT analysis and experimental findings. Greenish-yellow emission is exhibited by the fluorophores **BPy-1** and **BPy-2** in solution, solid-state, and thin-film matrices. However, **BPy-FL** exhibited blue emission in THF solution and greenish-yellow emission in the solid state with an absolute quantum yield of 93% attributable to both AIE and HLCT characteristics. When included in LED designs, the synthetic fluorophores act as organic downconverter materials for the LED and enhance the luminous stability and efficiency of the white LEDs. The fabricated white LEDs show excellent CRI values of more than 85 and warm white light emission with a CCT of ∼4000 K and a LER of ∼300 lm W^{-1}. Among them, the **BPy-FL**-based LED shows the highest CRI of 89. All the fluorophores are employed as acid–base vapor sensors because of the bipolar imidazole ring. The emission spectra reversibly switched between different colors (orange to yellow and blue to green) by frequent protonation and deprotonation. This characteristic enabled these probes to function as fluorescent pH sensors in both solution and solid states and to identify volatile organic molecules with high acidity. The protonation mechanism was also analyzed through NMR and DFT studies. Additionally, due to their intense greenish-yellow emissions and the AIE properties of the fluorophore **BPy-FL**, they are also used in anticounterfeiting LFP applications.

Data availability

The data supporting this article have been included as part of the ESI.†

Conflicts of interest

There are no conflicts to declare.

Acknowledgements

SP gratefully acknowledges ANRF, DST, Government of India for financial support through a power research grant (SPG/2023/000073). VS acknowledges ANRF, Department of Science and Technology (DST), India (CRG/2021/000494) and the Indian Institute of Technology Hyderabad, India (IITH/F324/2022-23/SG-138) for financial support.

References

1 K. R. Naveen, J. H. Oh, H. S. Lee and J. H. Kwon, Tailoring Extremely Narrow FWHM in Hypsochromic and Bathochromic Shift of Polycyclo-Heteraborin MR-TADF Materials for High-Performance OLEDs, *Angew. Chem., Int. Ed.*, 2023, **62**(32), e202306768, DOI: **10.1002/anie.202306768**.
2 S. Pimputkar, J. S. Speck, S. P. DenBaars and S. Nakamura, Prospects for LED Lighting, *Nat. Photonics*, 2009, **3**(4), 180–182, DOI: **10.1038/nphoton.2009.32**.

3 S. A. Patil, M. B. Budri, S. R. Inamdar and K. B. Gudasi, Effect of Hydroxyl Group on Photo-Physical Properties and Dipole Moments of Fluorescent Dyes: An Experimental and Computational Approach, *J. Fluoresc.*, 2023, **33**(3), 1041–1056, DOI: 10.1007/s10895-022-03105-y.

4 B. Dey, D. Boje, S. Giri and A. K. Atta, Bis-Pyrene-Containing Fluorescent Receptor for Explosive Picric Acid and Au(III) via Dynamic Excimer Quenching Process in Aqueous Medium: Practical Application, *J. Photochem. Photobiol., A*, 2024, **448**, 115293, DOI: 10.1016/j.jphotochem.2023.115293.

5 H. Zhang, J. Xue, C. Li, S. Zhang, B. Yang, Y. Liu and Y. Wang, Novel Deep-Blue Hybridized Local and Charge-Transfer Host Emitter for High-Quality Fluorescence/Phosphor Hybrid Quasi-White Organic Light-Emitting Diode, *Adv. Funct. Mater.*, 2021, **31**(25), 2100704, DOI: 10.1002/adfm.202100704.

6 J. D. Girase, J. H. Jou, S. Patel and S. Vaidyanathan, Solution-Processed Deep-Blue Fluorophores Based on Phenanthroimidazole Integrated with Benzimidazole with HLCT Character for Efficient Deep-Blue Organic Light Emitting Devices, *Dyes Pigm.*, 2022, **206**, 110623, DOI: 10.1016/j.dyepig.2022.110623.

7 Z. Wang, P. Lu, S. Chen, Z. Gao, F. Shen, W. Zhang, Y. Xu, H. S. Kwok and Y. Ma, Phenanthro[9,10-d]Imidazole as a New Building Block for Blue Light Emitting Materials, *J. Mater. Chem.*, 2011, **21**(14), 5451–5456, DOI: 10.1039/C1JM10321K.

8 B. P. Debata, M. D. Thiyagarajan, J. D. Girase, S. K. Iyer, S. Patel and S. Vaidyanathan, Benzil-Imidazole Blue Fluorophores and Their Applications in Blue/White Light-Emitting Diodes, Sensing and Anticounterfeiting, *J. Mater. Chem. C*, 2025, **13**(6), 2711–2731, DOI: 10.1039/D4TC04661G.

9 J. Tagare, D. K. Dubey, J.-H. Jou and S. Vaidyanathan, Synthesis, Photophysical, Theoretical and Electroluminescence Study of Triphenylamine-Imidazole Based Blue Fluorophores for Solution-Processed Organic Light Emitting Diodes, *Dyes Pigm.*, 2019, **160**, 944–956, DOI: 10.1016/j.dyepig.2018.09.007.

10 Y. Wang, C. Du, Z. Cheng, S. Ge, Z. Feng, L. Wan, Y. Hu, X. Ma, Z. Su and P. Lu, Rational Molecular Design of Phenanthroimidazole-Based Fluorescent Materials toward High-Efficiency Deep-Blue OLEDs by Molecular Isomer Engineering, *ACS Appl. Mater. Interfaces*, 2024, **16**(38), 51201–51211, DOI: 10.1021/acsami.4c05510.

11 B. P. Debata, J.-H. Jou, S. Patel and S. Vaidyanathan, The Design and Synthesis of 1-Phenylimidazo[1,5-a]Pyridine – Anthracene-Based Fluorophore for Greenish-Yellow Organic Light Emitting Diode and Warm White LED, *J. Inf. Disp.*, 2024, **25**(4), 1–13, DOI: 10.1080/15980316.2024.2304869.

12 S. R. Nayak, S. Patel and S. Vaidyanathan, Imidazole-Based Fluorescent Probes: Concomitant Effects of N1 Substitution and Lone Pair on Selective Recognition of Picric Acid, *New J. Chem.*, 2023, **47**(7), 3524–3534, DOI: 10.1039/D2NJ06079E.

13 D. C. Mukunda, V. K. Joshi and K. K. Mahato, Light Emitting Diodes (LEDs) in Fluorescence-Based Analytical Applications: A Review, *Appl. Spectrosc. Rev.*, 2022, **57**(1), 1–38, DOI: 10.1080/05704928.2020.1835939.

14 R. Devi and S. Vaidyanathan, Narrow Band Red Emitting Europium Complexes and Their Application in Smart White LEDs and Vapoluminescent Sensors, *Dalton Trans.*, 2020, **49**(19), 6205–6219, DOI: 10.1039/D0DT00519C.

15 C. Li, J. Wei, J. Han, Z. Li, X. Song, Z. Zhang, J. Zhang and Y. Wang, Efficient Deep-Blue OLEDs Based on Phenanthro[9,10-d]Imidazole-Containing Emitters with AIE and Bipolar Transporting Properties, *J. Mater. Chem. C*, 2016, **4**(42), 10120–10129, DOI: 10.1039/C6TC03923E.

16 N. Ruan, Q. Qiu, X. Wei, J. Liu, L. Wu, N. Jia, C. Huang and T. D. James, De Novo Green Fluorescent Protein Chromophore-Based Probes for Capturing Latent Fingerprints Using a Portable System, *J. Am. Chem. Soc.*, 2024, **146**(3), 2072–2079, DOI: 10.1021/jacs.3c11277.

17 M. Sun, M. Zhang, Y. Zhou, M. Xie, L. Chu, X. Wang, Q. Sun, F. Liu, W. Yang and S. Xue, Novel Electro-Fluorescent Materials with Hybridized Local and Charge-Transfer (HLCT) Excited State for Highly Efficient Non-Doped Pure Blue OLEDs, *Org. Chem. Front.*, 2023, **10**(6), 1485–1494, DOI: 10.1039/D2QO02039D.

18 S. Vaidyanathan and D. Y. Jeon, A novel narrow band red-emitting phosphor for white light emitting diodes, *Int. J. Appl. Ceram. Technol.*, 2009, **6**(4), 453–458.

19 L. Kang and Z. Lin, Regulation Strategy of White Emission from Organic–Inorganic Hybrid Metal Halide Perovskites, *Inorg. Chem. Front.*, 2023, **10**(1), 13–36, DOI: 10.1039/D2QI02076A.

20 S. Mund and S. Vaidyanathan, New Isomeric Ancillary Ligands and Their EuIII Complexes: A Single Component White Light Emissive Phosphor and Their Applications in Red/White Smart LEDs, Electronic Noses, and Temperature Sensing, *J. Mater. Chem. C*, 2022, **10**(18), 7201–7215, DOI: 10.1039/D2TC00664B.

21 Y. Narukawa, I. Niki, K. Izuno, M. Yamada, Y. Murazaki and T. Mukai, Phosphor-Conversion White Light Emitting Diode Using InGaN Near-Ultraviolet Chip, *Jpn. J. Appl. Phys.*, 2002, **41**(4A), L371, DOI: 10.1143/JJAP.41.L371.

22 S. P. DenBaars, D. Feezell, K. Kelchner, S. Pimputkar, C.-C. Pan, C.-C. Yen, S. Tanaka, Y. Zhao, N. Pfaff, R. Farrell, M. Iza, S. Keller, U. Mishra, J. S. Speck and S. Nakamura, Development of Gallium-Nitride-Based Light-Emitting Diodes (LEDs) and Laser Diodes for Energy-Efficient Lighting and Displays, *Acta Mater.*, 2013, **61**(3), 945–951, DOI: 10.1016/j.actamat.2012.10.042.

23 P. Pust, P. J. Schmidt and W. Schnick, A Revolution in Lighting, *Nat. Mater.*, 2015, **14**(5), 454–458, DOI: 10.1038/nmat4270.

24 S. Tonzani, Lighting Technology: Time to Change the Bulb, *Nature*, 2009, **459**(7245), 312–314, DOI: 10.1038/459312a.

25 C. Lee, C. Shen, C. Cozzan, R. M. Farrell, J. S. Speck, S. Nakamura, B. S. Ooi and S. P. DenBaars, Gigabit-per-Second White Light-Based Visible Light Communication Using near-Ultraviolet Laser Diode and Red-, Green-, and Blue-Emitting Phosphors, *Opt. Express*, 2017, **25**(15), 17480–17487, DOI: 10.1364/OE.25.017480.

26 A. Luridiana, G. Pretta, D. Chiriu, C. M. Carbonaro, R. Corpino, F. Secci, A. Frongia, L. Stagi and P. C. Ricci, A Facile Strategy for New Organic White LED Hybrid Devices: Design, Features and Engineering, *RSC Adv.*, 2016, **6**(26), 22111–22120, DOI: **10.1039/C6RA00999A**.

27 T.-H. Han, Y. Lee, M.-R. Choi, S.-H. Woo, S.-H. Bae, B. H. Hong, J.-H. Ahn and T.-W. Lee, Extremely Efficient Flexible Organic Light-Emitting Diodes with Modified Graphene Anode, *Nat. Photonics*, 2012, **6**(2), 105–110, DOI: **10.1038/nphoton.2011.318**.

28 J. He, Y. Wang, R. Li, X. Yuan, S. Xu and L. Zhang, Tunable and White Light Emitting AlPO4 Mesoporous Glass by Design of Inorganic/Organic Luminescent Species, *APL Mater.*, 2015, **3**(4), 46101, DOI: **10.1063/1.4916697**.

29 D. Di Martino, L. Beverina, M. Sassi, S. Brovelli, R. Tubino and F. Meinardi, Straightforward Fabrication of Stable White LEDs by Embedding of Inorganic UV-LEDs into Bulk Polymerized Polymethyl-Methacrylate Doped with Organic Dyes, *Sci. Rep.*, 2014, **4**(1), 4400, DOI: **10.1038/srep04400**.

30 M. Mosca; R. Macaluso and I. Crupi, Hybrid Inorganic–Organic White Light Emitting Diodes, in *Polymers for Light-Emitting Devices and Displays*, 2020, pp. 197–262. , DOI: **10.1002/9781119654643.ch8**.

31 A. Luridiana, G. Pretta, D. Chiriu, C. M. Carbonaro, R. Corpino, F. Secci, A. Frongia, L. Stagi and P. C. Ricci, A Facile Strategy for New Organic White LED Hybrid Devices: Design, Features and Engineering, *RSC Adv.*, 2016, **6**(26), 22111–22120, DOI: **10.1039/C6RA00999A**.

32 B. Rajamouli, P. Sood, S. Giri, V. Krishnan and V. Sivakumar, A Dual-Characteristic Bidentate Ligand for a Ternary Mononuclear Europium(III) Molecular Complex – Synthesis, Photophysical, Electrochemical, and Theoretical Study, *Eur. J. Inorg. Chem.*, 2016, 3900–3911, DOI: **10.1002/ejic.201600508**.

33 J. Tagare, H. Ulla, M. N. Satyanarayan and S. Vaidyanathan, Synthesis, Photophysical and Electroluminescence Studies of New Triphenylamine-Phenanthroimidazole Based Materials for Organic Light Emitting Diodes, *J. Lumin.*, 2018, **194**, 600–609, DOI: **10.1016/j.jlumin.2017.09.020**.

34 E. Angioni, R. J. Marshall, N. J. Findlay, J. Bruckbauer, B. Breig, D. J. Wallis, R. W. Martin, R. S. Forgan and P. J. Skabara, Implementing Fluorescent MOFs as Down-Converting Layers in Hybrid Light-Emitting Diodes, *J. Mater. Chem. C*, 2019, **7**(8), 2394–2400, DOI: **10.1039/C9TC00067D**.

35 K. Singh and S. Vaidyanathan, Synthesis and Optical Properties of New Red Emitting Phosphor Li3BaSrGd3-xEux (MO4) 8 for White LEDs, *ChemistrySelect*, 2016, **1**(17), 5448–5462.

36 R. Boddula, J. Tagare, K. Singh and S. Vaidyanathan, White Light-Emissive Europium Complexes and Their Versatile Applications, *Mater. Chem. Front.*, 2021, **5**(7), 3159–3175, DOI: **10.1039/D1QM00083G**.

37 S. Mund, K. Singh, M. Panda, B. K. Biswal, U. Subuddhi and S. Vaidyanathan, Thiabendazole: A New Class of Antenna Core Structure for Multifunctional Trivalent Organo-Europium (EuIII) Complexes, *J. Mater. Chem. C*, 2022, **10**(29), 10645–10659, DOI: **10.1039/D2TC01078J**.

38 C.-H. Chen, W.-S. Huang, M.-Y. Lai, W.-C. Tsao, J. T. Lin, Y.-H. Wu, T.-H. Ke, L.-Y. Chen and C.-C. Wu, Versatile, Benzimidazole/Amine-Based Ambipolar Compounds for Electroluminescent Applications: Single-Layer, Blue, Fluorescent OLEDs, Hosts for Single-Layer, Phosphorescent OLEDs, *Adv. Funct. Mater.*, 2009, **19**(16), 2661–2670, DOI: **10.1002/adfm.200900561**.

39 D. Di Martino, L. Beverina, M. Sassi, S. Brovelli, R. Tubino and F. Meinardi, Straightforward Fabrication of Stable White LEDs by Embedding of Inorganic UV-LEDs into Bulk Polymerized Polymethyl-Methacrylate Doped with Organic Dyes, *Sci. Rep.*, 2014, **4**(1), 4400, DOI: **10.1038/srep04400**.

40 M. Sun, C. Zeng, W. Liu, M. Xu, L. Bu, E. Zhang, K. Chen, J. Liu, W. Zhao and M. Ding, Facile Synthesis and Tunable Fluorescent Properties of a New D-π-A Isocoumarin: Applications in Encryption and OLED Technology, *J. Mol. Struct.*, 2025, **1321**, 140173, DOI: **10.1016/j.molstruc.2024.140173**.

41 Y. Zhu, K. Liao, Y. Li, W. Zhang, B. Song, X.-Q. Hao and X. Zhu, Dual-State Emissive Imidazo[1,2-α]Pyridines with Full Color Emission, Acidochromism, Viscosity-Dependent Fluorescence, and Bioimaging Applications, *Dyes Pigm.*, 2024, **224**, 112004, DOI: **10.1016/j.dyepig.2024.112004**.

42 S. Gadiyaram, A. Ghosh, V. D. Ghule, P. K. Sharma and D. Amilan Jose, Aggregation-Induced Emission Active Multianalyte Sensor: Detection of PH, Carbonate, Bi-Carbonate and Nitroaromatics in Water, *Microchem. J.*, 2024, **204**, 110957, DOI: **10.1016/j.microc.2024.110957**.

43 P. R. Lakshmi, B. Mohan, P. Kang, P. Nanjan and S. Shanmugaraju, Recent Advances in Fluorescence Chemosensors for Ammonia Sensing in the Solution and Vapor Phases, *Chem. Commun.*, 2023, **59**(13), 1728–1743, DOI: **10.1039/D2CC06529K**.

44 V. Schmitt, S. Moschel and H. Detert, Diaryldistyrylpyrazines: Solvatochromic and Acidochromic Fluorophores, *Eur. J. Org. Chem.*, 2013, 5655–5669, DOI: **10.1002/ejoc.201300463**.

45 S. Kothavale and N. Sekar, Novel Pyrazino-Phenanthroline Based Rigid Donor-π-Acceptor Compounds: A Detail Study of Optical Properties, Acidochromism, Solvatochromism and Structure-Property Relationship, *Dyes Pigm.*, 2017, **136**, 31–45, DOI: **10.1016/j.dyepig.2016.08.032**.

46 R. K. Jain, D. Sunil and P. Bhagavath, Organic Fluorophores in Developing Latent Fingerprints: An up-to-Date Review, *J. Coatings Technol. Res.*, 2025, **22**(1), 117–147, DOI: **10.1007/s11998-024-00991-8**.

47 N. K. Durgi and P. P. Pujar, Solid-State Organic Fluorophore for Latent Fingerprint Detection and Anti-Counterfeiting Applications, *ChemistrySelect*, 2024, **9**(2), e202304066, DOI: **10.1002/slct.202304066**.

48 H. Irshad, Khadija and K. Qvortrup, Novel AIE and Solvatochromism Exhibiting TPE Based Organic Fluorophore with Excellent Emission Properties in Solid and Solution Phase for Latent Fingerprint and Metronidazole Sensing in Real Samples, *J. Mol. Liq.*, 2024, **414**, 126049, DOI: **10.1016/j.molliq.2024.126049**.

49 M. Ahmad, G. Kumar, V. Luxami, S. Kaur, P. Singh and S. Kumar, Fluorescence Imaging of Surface-Versatile Latent

Fingerprints at the Second and Third Level Using Double ESIPT-Based AIE Fluorophore, *New J. Chem.*, 2021, **45**(17), 7705–7713, DOI: **10.1039/D1NJ00678A**.

50 S. Zhang, R. Liu, Q. Cui, Y. Yang, Q. Cao, W. Xu and L. Li, Ultrabright Fluorescent Silica Nanoparticles Embedded with Conjugated Oligomers and Their Application in Latent Fingerprint Detection, *ACS Appl. Mater. Interfaces*, 2017, **9**(50), 44134–44145, DOI: **10.1021/acsami.7b15612**.

51 D.-D. Xie, H.-S. Liao, Y.-H. Jian, D. Chen, H.-J. Chi, B.-Y. Wang, Y.-L. Lv, Y. Dong and X. Li, Achieving High-Performance Non-Doped Sky-Blue OLEDs with Negligible Efficiency Roll-off by Combining AIE, HLCT and Mechanoluminescence Features, *Dyes Pigm.*, 2023, **209**, 110951, DOI: **10.1016/j.dyepig.2022.110951**.

52 C. Chaiwai, W. Kitisriworaphan, S. Petdee, P. Nalaoh, T. Chawanpunyawat, P. Chasing, T. Manyum, T. Sudyoadsuk and V. Promarak, Solid-State Fluorophores Featuring a Combined Hybridized Local and Charge Transfer Excited State and Aggregation-Induced Emission as Efficient Emitters for Electroluminescent Devices, *Dyes Pigm.*, 2023, **216**, 111311, DOI: **10.1016/j.dyepig.2023.111311**.

53 N. A. Kukhta and M. R. Bryce, Dual Emission in Purely Organic Materials for Optoelectronic Applications, *Mater. Horiz.*, 2021, **8**(1), 33–55, DOI: **10.1039/D0MH01316A**.

54 J. Fan, Y. Zhang, K. Zhang, J. Liu, G. Jiang, F. Li, L. Lin and C.-K. Wang, Towards Boosting the Exciton Lifetime and Efficiency of Near-Infrared Aggregation Induced Emitters with Hybridized Local and Charge Transfer Excited States: A Multiscale Study, *J. Mater. Chem. C*, 2019, **7**(29), 8874–8887, DOI: **10.1039/C9TC02144B**.

55 D. V. Berdnikova, S. Steup, M. Bolte and M. Suta, Design of Aurone-Based Dual-State Emissive (DSE) Fluorophores, *Chem. – A Eur. J.*, 2023, **29**(27), e202300356, DOI: **10.1002/chem.202300356**.

56 J. L. Belmonte-Vázquez, Y. A. Amador-Sánchez, L. A. Rodríguez-Cortés and B. Rodríguez-Molina, Dual-State Emission (DSE) in Organic Fluorophores: Design and Applications, *Chem. Mater.*, 2021, **33**(18), 7160–7184, DOI: **10.1021/acs.chemmater.1c02460**.

57 J. Devesing Girase, S. Mukherjee, T. Chakrabarti, S. Patel, A. Perumal and S. Vaidyanathan, Mild Donor-π-Mild Acceptor (MD-π-MA) Benzimidazole-Based Deep Blue Fluorophores with Hybridized Local and Charge Transfer (HLCT) Excited States for OLEDs, *J. Inf. Disp.*, 2022, **23**(3), 221–234, DOI: **10.1080/15980316.2022.2075042**.

58 M. K. Ravindra, G. P. Darshan, D. R. Lavanya, K. M. Mahadevan, H. B. Premkumar, S. C. Sharma, H. Adarsha and H. Nagabhushana, Aggregation Induced Emission Based Active Conjugated Imidazole Luminogens for Visualization of Latent Fingerprints and Multiple Anticounterfeiting Applications, *Sci. Rep.*, 2021, **11**(1), 16748, DOI: **10.1038/s41598-021-96011-5**.

59 S. R. Nayak, J. D. Girase, M. R. Nagar, J.-H. Jou and S. Vaidyanathan, Solution Processable Deep-Blue OLEDs Based on Benzimidazole-TPA Conjugated through 9,9-Diethyl Fluorene (D-π-A) Luminophore with a Hybridized Local and Charge Transfer Excited State, *J. Phys. Chem. C*, 2023, **127**(21), 10291–10302, DOI: **10.1021/acs.jpcc.3c00790**.

60 Z. Chen, J. Zhang, M. Song, J. Yin, G.-A. Yu and S. H. Liu, A Novel Fluorene-Based Aggregation-Induced Emission (AIE)-Active Gold(i) Complex with Crystallization-Induced Emission Enhancement (CIEE) and Reversible Mechanochromism Characteristics, *Chem. Commun.*, 2015, **51**(2), 326–329, DOI: **10.1039/C4CC08087D**.

61 J. D. Girase, Shahnawaz, J.-H. Jou and S. Vaidyanathan, Deep-Blue Fluorophores Based on Phenanthroimidazole Integrated with Benzo[d]Thiazole: Experimental and Theoretical Investigation, *ChemistrySelect*, 2022, **7**(27), e202201514, DOI: **10.1002/slct.202201514**.

62 J. D. Girase, S. Singh, B. P. Debata, S. R. Nayak, M. R. Nagar, J.-H. Jou, S. Patel and S. Vaidyanathan, Structural Engineering of Deep-Blue Emitters (Imidazoles Integrated with Triphenylamine) Leads to EQE > 6% and High Color Purity (CIEy ∼ 0.09) for Solution-Processed OLEDs, *J. Phys. Chem. C*, 2023, **127**(33), 16623–16635, DOI: **10.1021/acs.jpcc.3c03058**.

63 Y. Kim, H. M. Hwang, L. Wang, I. Kim, Y. Yoon and H. Lee, Solar-Light Photocatalytic Disinfection Using Crystalline/Amorphous Low Energy Bandgap Reduced TiO2, *Sci. Rep.*, 2016, **6**(1), 25212, DOI: **10.1038/srep25212**.

64 C. He, H. Guo, Q. Peng, S. Dong and F. Li, Asymmetrically Twisted Anthracene Derivatives as Highly Efficient Deep-Blue Emitters for Organic Light-Emitting Diodes, *J. Mater. Chem. C*, 2015, **3**(38), 9942–9947, DOI: **10.1039/C5TC02055G**.

65 H. Li, Y. Guo, G. Li, H. Xiao, Y. Lei, X. Huang, J. Chen, H. Wu, J. Ding and Y. Cheng, Aggregation-Induced Fluorescence Emission Properties of Dicyanomethylene-1,4-Dihydropyridine Derivatives, *J. Phys. Chem. C*, 2015, **119**(12), 6737–6748, DOI: **10.1021/jp511060k**.

66 Y. Zhen, F. Zhang, H. Liu, Y. Yan, X. Li and S. Wang, Impact of Peripheral Groups on Pyrimidine Acceptor-Based HLCT Materials for Efficient Deep Blue OLED Devices, *J. Mater. Chem. C*, 2022, **10**(27), 9953–9960, DOI: **10.1039/D2TC01766K**.

67 M. Sun, C. Ma, M. Xie, L. Chu, Q. Sun, W. Yang and S. Xue, Highly Efficient Deep Blue Electroluminescent Material with High and towards Balanced Carrier Transmission Performance Based on Hybrid Local and Charge-Transfer (HLCT) Excited State, *Chem. Eng. J.*, 2024, **480**, 148107, DOI: **10.1016/j.cej.2023.148107**.

68 J. D. Girase, M. R. Nagar, Shahnawaz, A. Choudhury, J.-H. Jou and S. Vaidyanathan, Highly Efficient Multifunctional Luminogens for Near UV/Deep Blue (CIEy ∼0.02) and Hybrid White OLEDs (CIE ∼0.33, 0.37) with Superior Color Stability, *ACS Appl. Electron. Mater.*, 2022, **4**(9), 4368–4382, DOI: **10.1021/acsaelm.2c00648**.

69 S. R. Nayak, Shahnawaz, I. Siddiqui, J.-H. Jou, S. Patel and S. Vaidyanathan, Multifunctional 4,5-Diphenyl-1H-Imidazole-Based Luminogens as Near UV/Deep Blue Emitters/Hosts for Organic Light-Emitting Diodes and Selective Picric Acid Detection, *J. Phys. Chem. C*, 2023, **127**(1), 499–515, DOI: **10.1021/acs.jpcc.2c05220**.

70 M. I. Alam, M. R. Nagar, D. Barman, P. K. Iyer, J.-H. Jou and S. Vaidyanathan, Tailoring Structural Rigidity Utilizing a Lock/Unlock Donor Strategy for Highly Efficient Solution Processed Blue and Green HLCT OLEDs, *J. Mater. Chem. C*, 2024, **12**(34), 13585–13595, DOI: 10.1039/D4TC00417E.

71 M. I. Alam, M. R. Nagar, J.-H. Jou and S. Vaidyanathan, Twisted Acceptor Core Molecular Design with Phenoxazine and Phenothiazine Donors Enabled Yellow Thermally Activated Delayed Fluorescent Emitters/Sensitizers for Long-Lifetime Solution-Processed Organic Light-Emitting Diodes Exceeding 31% External Quantum, *Chem. Mater.*, 2024, **36**(18), 8649–8662, DOI: 10.1021/acs.chemmater.4c01001.

72 A. Liu, Q. Zhang, L. Pan, F. Yang, D. Lin and C. Jiang, Donor–Acceptor Type Solvatochromic Flavonoid Materials Fluorphores for Polarity Sensing and Real-Time Temperature Monitoring, *Adv. Funct. Mater.*, 2024, 2415250, DOI: 10.1002/adfm.202415250.

73 M. S. Filho, E. S. Moraes, L. C. da Luz, F. da Silveira Santos, A. R. Martin, R. Benhida, L. G. T. A. Duarte and F. S. Rodembusch, Synthesis, Photophysics, and Theoretical Calculations of Styryl-Based Fluorophores Harboring Substituted Benzothiazole Acceptors, *J. Photochem. Photobiol., A*, 2023, **435**, 114287, DOI: 10.1016/j.jphotochem.2022.114287.

74 J. Tagare and S. Vaidyanathan, Recent Development of Phenanthroimidazole-Based Fluorophores for Blue Organic Light-Emitting Diodes (OLEDs): An Overview, *J. Mater. Chem. C*, 2018, **6**(38), 10138–10173, DOI: 10.1039/C8TC03689F.

75 J. Devesing Girase, S. Rani Nayak, J. Tagare, Shahnawaz, M. Ram Nagar, J.-H. Jou and S. Vaidyanathan, Solution-Processed Deep-Blue (Y ~ 0.06) Fluorophores Based on Triphenylamine-Imidazole (Donor-Acceptor) for OLEDs: Computational and Experimental Exploration, *J. Inf. Disp.*, 2022, **23**(1), 53–67, DOI: 10.1080/15980316.2021.1959429.

76 S. Kumar, S. K. Jain and R. C. Rastogi, An Experimental and Theoretical Study of Excited-State Dipole Moments of Some Flavones Using an Efficient Solvatochromic Method Based on the Solvent Polarity Parameter, ETN, *Spectrochim. Acta, Part A*, 2001, **57**(2), 291–298, DOI: 10.1016/S1386-1425(00)00372-3.

77 A. Varghese and K. B. Akshaya, *Application of Fluorescence in Solvatochromic Studies of Organic Compounds BT - Reviews in Fluorescence*, ed. Geddes, C. D., Springer International Publishing, Cham, 2017, pp. 99–121, DOI: 10.1007/978-3-030-01569-5_5.

78 S. Mund, K. Singh, T. Deepak, A. R. Babu, U. Subuddhi and S. Vaidyanathan, Unveiling the Versatility of Coumarin-Integrated with Phenanthroline/Thiabendazole-Based EuIII Complexes for Smart LEDs, Vapoluminescence, and Bioimaging Applications, *ACS Appl. Bio Mater.*, 2024, **7**(9), 5795–5809, DOI: 10.1021/acsabm.4c00839.

79 M. Rajendran, R. Devi, S. Mund, K. Singh and S. Vaidyanathan, Energy Transfer Cooperation between Ligands and EuIII Ions in Molecular Europium Complexes for Vapoluminescence Sensing (Reversible on/off Emission Switching) and Hybrid White LED/Plant-Growth Applications, *J. Mater. Chem. C*, 2021, **9**(42), 15034–15046, DOI: 10.1039/D1TC02363B.

80 O. Anitha, M. Mathivanan, B. Tharmalingam, T. Thiruppathiraja, S. Ghorai, R. Natarajan, V. Thiagarajan, S. Lakshmipathi and B. Murugesapandian, Multi-Stimuli Responsiveness of Pyrimidine Bishydrazone: AIE, Tuneable Luminescence, White Light Emission, Mechanochromism, Acidochromism and Its Anticounterfeiting Applications, *Dyes Pigm.*, 2023, **212**, 111091, DOI: 10.1016/j.dyepig.2023.111091.

81 W. Qu, Z. Gao, X. Fan, X. Tian, H. Wang and B. Wei, Organic Fluorescent Compounds with Twisted D-π-A Molecular Structure and Acidochromic Properties, *J. Mol. Struct.*, 2022, **1260**, 132831, DOI: 10.1016/j.molstruc.2022.132831.

82 C. Zeng, T. Yang, Z. Wang, K. Chen, Q. Ge, W. Peng, J. Zhang, J. Liu, T. Zhang and M. Sun, Functional-Group-Regulated Stimuli-Responsive Banana-Shaped α-Cyanostilbene Derivatives: Dual-State Emission, AIEE, Acidochromism and Their Applications in Anti-Counterfeiting, Fingerprint Recognition and OLEDs, *J. Lumin.*, 2024, **269**, 120452, DOI: 10.1016/j.jlumin.2024.120452.

83 X. Xin, Y. Jing, P. Li, X. Zhang, J. Li, L. Li and L. Zhang, Imidazole-Based Metal–Organic Framework for the ''On1–Off–On2'' Fluorescence-Based Detection of Picric Acid and the Adsorption of Congo Red, *Cryst. Growth Des.*, 2023, **23**(6), 3988–3995, DOI: 10.1021/acs.cgd.2c01186.

84 N. N. M. Y. Chan, A. Idris, Z. H. Z. Abidin and H. A. Tajuddin, White Light Emission from Coumarin and Rhodamine Derivatives Based on RGB Multicomponent System, *J. Photochem. Photobiol., A*, 2023, **439**, 114577, DOI: 10.1016/j.jphotochem.2023.114577.